

1 This is a non-peer reviewed preprint submitted to EarthArXiv. This is preprint v2.

2 **Mapping Europe's Natural Hydrogen Potential: A Continental-Scale**
3 **Geological Prospectivity Assessment**

4 Florian H. J. Willemse¹, Johannes M. Miocic^{1*}

5 ¹GeoEnergy, Energy and Sustainability Research Institute Groningen, University of Groningen,
6 Nijenborgh 6, 9747 AG Groningen, the Netherlands

7 *Corresponding author: j.m.miocic@rug.nl

8

9 **Abstract**

10 Natural hydrogen, generated by a range of geological processes in the Earth's crust, is emerging
11 as a promising carbon-neutral energy source. However, systematic large-scale assessments of
12 its subsurface occurrence remain limited. This study presents the first continental-scale
13 prospectivity map of natural hydrogen in Europe, integrating geological indicators of hydrogen
14 generation, reservoir quality, and sealing capacity. A comprehensive inventory of ultramafic rock
15 bodies—key indicators of hydrogen potential—is compiled and spatially analysed. To address
16 geological uncertainty, we apply Monte Carlo simulations, yielding conservative, median, and
17 optimistic resource estimates. High-prospectivity regions are identified in Hungary, Denmark,
18 Poland, and Serbia, with many documented hydrogen occurrences aligning with predicted
19 source zones. This spatial assessment provides a critical framework for early-stage exploration,
20 supports future energy security strategies, and highlights key regions for focused research and
21 development in the context of the energy transition.

22

23 **Keywords:** Natural hydrogen; Prospectivity mapping; Serpentinitization; Radiolysis; Ultramafic
24 rocks; Geological exploration; Monte Carlo simulation; Energy transition; Europe

25

26

27 **1. Introduction**

28 The global transition to carbon-neutral, renewable-based energy systems is essential to mitigate
29 the effects of climate change and limit global warming (Rogelj et al., 2015). The configuration of
30 regional decarbonized energy systems depends not only on the spatial distribution and
31 availability of renewable energy sources but also on demand profiles, infrastructure
32 interconnectivity, and the suitability of specific energy carriers for various applications. Among
33 these carriers, hydrogen has received growing attention due to its versatility in sectors such as
34 transportation, industry, and energy storage (Hanley et al., 2018; McPherson et al., 2018). Despite
35 this potential, over 95% of hydrogen currently in use is derived from fossil fuels, leading to
36 considerable carbon dioxide emissions (IRENA, 2023). Key barriers to scaling up low-carbon
37 hydrogen include the high cost of green hydrogen production and the competitiveness of other
38 renewable-based technologies for many applications (Liebreich et al., 2023).

39 In this context, natural hydrogen—also known as *white* or *gold* hydrogen—is emerging as a
40 promising, potentially low-cost and low-emission alternative. Generated by geological processes
41 such as serpentinization, radiolysis, and iron oxidation within the Earth’s crust, natural hydrogen
42 has long been observed at surface seeps, particularly in tectonic and mid-ocean ridge settings.
43 However, early assessments dismissed the likelihood of significant subsurface accumulations
44 due to the gas’s high diffusivity and reactivity (USGS, 1993; Zgonnik et al., 2015).

45 Renewed interest in the last two decades (Smith et al., 2005; Zgonnik, 2020) has been driven by
46 growing evidence that natural hydrogen may occur more broadly than previously believed. Recent
47 estimates suggest that the subsurface generation of hydrogen may amount to thousands to
48 billions of megatons globally (Ellis & Gelman, 2024). However, the economic viability of these
49 resources remains uncertain, depending heavily on depth, geological setting, and the physical
50 state of the hydrogen—whether free gas or dissolved in formation waters. Cost estimates vary
51 widely: some studies suggest that natural hydrogen could be more affordable than both green
52 and grey hydrogen (Rigollet & Prinzhofe, 2022), while others express scepticism regarding
53 scalability and accessibility (Patonia et al., 2024). Similarly, the question whether natural H₂
54 could be considered renewable is disputed, with some indicating that it may not be (Brunet &
55 Malvoisin, 2025).

56 Effective exploration is therefore essential to assess the distribution and extractability of natural
57 hydrogen. Existing detection methods, such as soil gas sampling, are spatially limited and often
58 ambiguous in distinguishing active hydrogen seeps from background signals (Lévy et al., 2023;
59 Aimar et al., 2023). In response, geologically based prospectivity assessments have been
60 proposed to prioritize areas for more detailed investigation. One such effort is the recent
61 prospectivity mapping of the United States by Gelman et al. (2023), which incorporated indicators
62 of hydrogen sources, reservoirs, and seals.

63 In this study, we apply a similar methodology to construct the first continent-wide natural
64 hydrogen prospectivity map for Europe. We integrate multiple geological datasets, including a
65 comprehensive inventory of ultramafic complexes and updated records of hydrogen
66 occurrences—some previously undocumented. Unlike earlier regional studies (e.g., Donzé et al.,
67 2024; Gaucher et al., 2023), our work offers a systematic assessment of hydrogen generation
68 potential at the continental scale. By addressing geological uncertainty through Monte Carlo

69 simulations, we provide conservative, median, and optimistic resource estimates. This work aims
70 to support the strategic exploration of natural hydrogen resources in Europe and to contribute to
71 the continent's broader goals of energy transition and resilience.

72 **2. Methodology**

73 To identify regions with high natural hydrogen prospectivity, geological indicators related to
74 hydrogen sources, reservoirs, and seals were integrated using GIS software (QGIS). The selected
75 indicators are listed in Table 1, and their presence was determined based on publicly available
76 geological datasets (e.g., EGDI, IGME) and relevant literature. Following the methodology
77 developed by Gelman et al. (2025), each indicator was assigned a chance of sufficiency (COS)
78 value. The COS represents the fractional probability that a given feature is both present and
79 effective in contributing to hydrogen accumulation. These values were established by a panel of
80 experts, and where indicators overlap with those used in Gelman et al. (2025), the same COS
81 values and spatial buffers were adopted. This approach results in a relative prospectivity score—
82 not a statistical probability—that allows for comparison across regions at a continental scale. It
83 is particularly suited to early-stage exploration where data constraints preclude precise
84 quantification. Details of the calculation procedures for composite layers are provided in
85 Supplementary Material C.2.

86 To account for geological uncertainty, Monte Carlo simulations ($n = 1,000$) were performed by
87 sampling COS values from triangular probability distributions defined by low, median (mode),
88 and high estimates for each indicator (Table 1). This yields P10, P50, and P90 maps representing
89 optimistic, median, and conservative prospectivity scenarios, respectively. P50 maps are
90 presented in the main text, while P10 and P90 maps are included in Supplementary Material B.

91 **Table 1 | Geological indicators included in the prospectivity analysis, and chance of sufficiency (COS)**
92 values for each layer, used in the uncertainty analysis (triangular distribution Monte Carlo simulation).

93 *Buffer is given a larger radius based on the size of the uranium deposit, see *Supplementary Material C.1*.

Layer	COS low	COS med	COS high	Spatial buffer
Serpentinization (SER)				
SER1 - Ultramafic rocks (-)	0.5	0.6	0.7	20 km
SER2 - Ultramafic rocks (o)	0.6	0.7	0.8	20 km
SER3 - Ultramafic rocks (+)	0.7	0.8	0.9	20 km
SER4 - Isostatic gravity	0.1	0.4	0.7	-
SER5 - Failed rifts	0.7	0.8	0.9	-
SER6 - Rift-inversion orogens	0.7	0.8	0.9	-
SER7 - Banded iron formations	0.6	0.7	0.8	20 km
SER8 - Every other area	0	0.1	0.2	-
Radiolysis (RAD)				
RAD1 – Uranium occurrence	0.1	0.2	0.3	Varies*
RAD2 - Precambrian craton	0.5	0.7	0.9	100 km
RAD3 - Accreted terranes	0.1	0.2	0.5	100 km
Deep source (DEE)				
DEE1 - Faults	0.1	0.2	0.3	10 km
DEE2 - Suture zones	0.2	0.5	0.8	40 km
DEE3 - High heat flow	0.5	0.7	0.9	-
DEE4 - Heat flow buffer	0.1	0.2	0.3	-

DEE5 - Every other area	0	0.1	0.2	-
Reservoir (RES)				
RES1 - Sedimentary rocks	0.8	0.95	1	-
RES2 - Igneous / Metamorphic rocks	0.7	0.8	0.9	-
RES3 - Sedimentary basins	1	1	1	-
Seal (SEA)				
SEA1 - Subsurface salt	0.9	0.95	1	-
SEA2 - Sedimentary rocks	0.6	0.8	1	-
SEA3 - Igneous / Metamorphic rocks	0.2	0.5	0.8	-
SEA4 - Sedimentary basins	0.1	0.3	0.5	-

94

95

3. Results

96

3.1 Sources of natural hydrogen

97

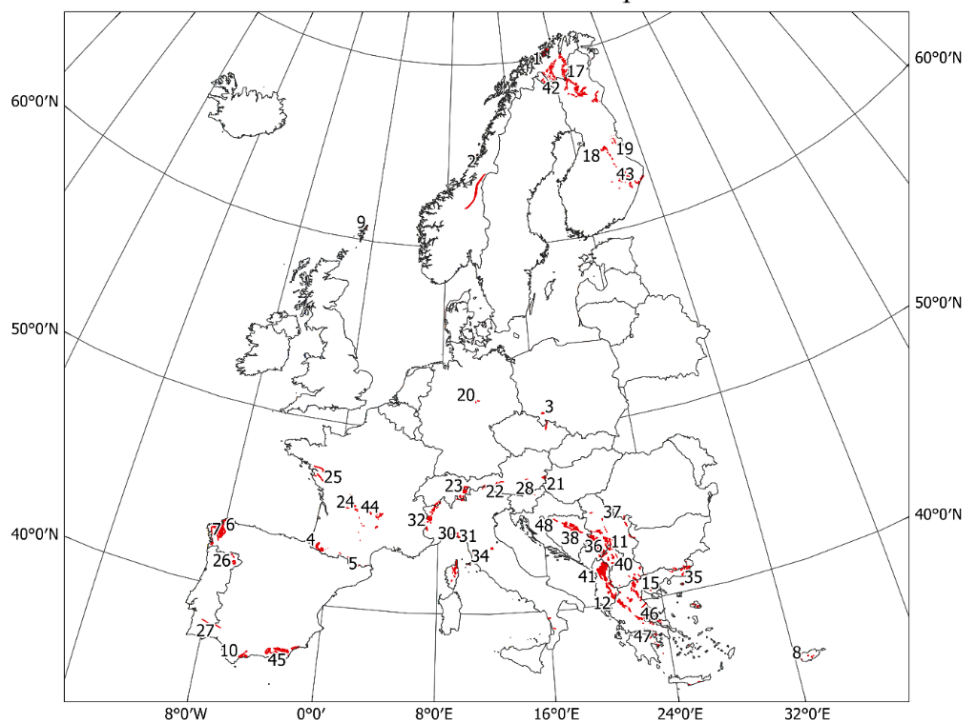
3.1.1 Serpentinisation

98 Hydrogen can be produced through serpentinization, a geochemical reaction involving the
 99 hydration of ultramafic rocks—typically rich in iron and low in silica—by water. As ultramafic
 100 rocks are key precursors for this process, their distribution serves as a primary indicator of
 101 hydrogen generation potential.

102 Due to the lack of a comprehensive ultramafic rock dataset for Europe, a compilation of ophiolitic
 103 complexes was used as a proxy. Ophiolites—tectonically emplaced fragments of oceanic
 104 lithosphere—often contain ultramafic rocks derived from the Earth's upper mantle. However, not
 105 all ophiolites contain ultramafic material, and not all ultramafic rocks are ophiolitic in origin (Zuo
 106 et al., 2022; Pomonis & Maggnas, 2017). Therefore, a systematic literature review was
 107 conducted to verify the composition of individual ophiolites and to identify additional, non-
 108 phiolitic ultramafic bodies. This included analysis of geomagnetic data, cross-sections, and
 109 petrological studies. A complete list of identified ultramafic occurrences is provided in Table A1
 110 (Supplementary Material).

111 Depth is also a critical factor: serpentinization is most efficient between depths of approximately
 112 4 to 21 km, depending on the geothermal gradient (Zgonnik, 2020; Criss, 2019). Accordingly, each
 113 occurrence was classified based on depth constraints and assigned a COS value: high (SER3, '+'),
 114 medium (SER2, 'o'), or low (SER1, '-'). Figure 1 shows the mapped ultramafic bodies and ophiolite
 115 complexes, labeled according to Table A1. These occurrences are concentrated in orogenic
 116 zones such as the Alps.

Ultramafic Rocks of Europe



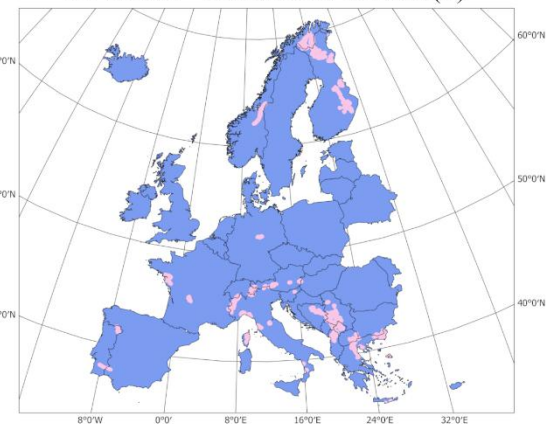
117

118 **Figure 1** | Distribution of ultramafic bodies and ophiolitic complexes across Europe. Labels correspond to
119 entries in Table A1. Only ophiolites confirmed to contain ultramafic material are included.

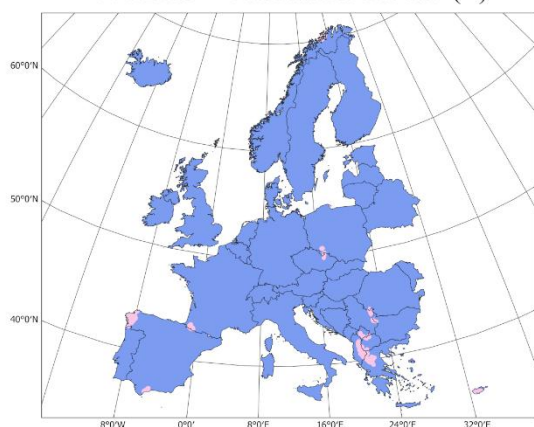
A. SER1 - Ultramafic Rocks (-)



B. SER2 - Ultramafic Rocks (o)



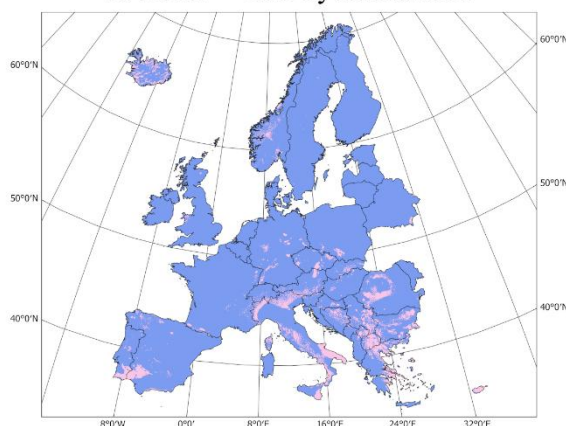
C. SER3 - Ultramafic Rocks (+)



D. SER4 - Failed Rifts



E. SER5 - Gravity Anomalies



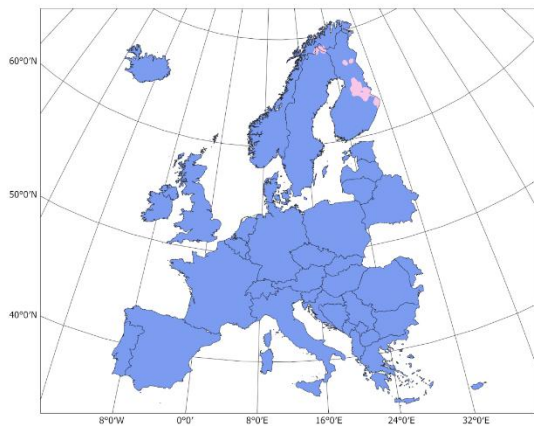
Presence
 No presence

120

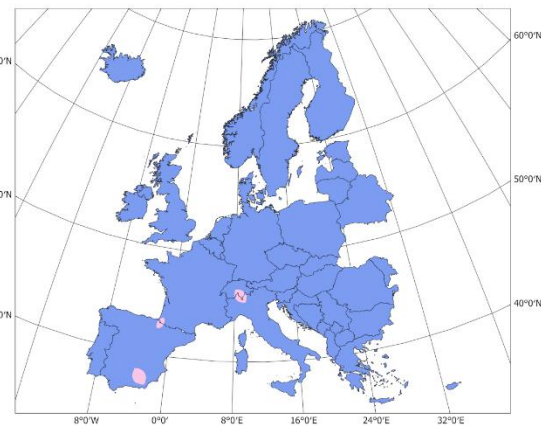
121

122

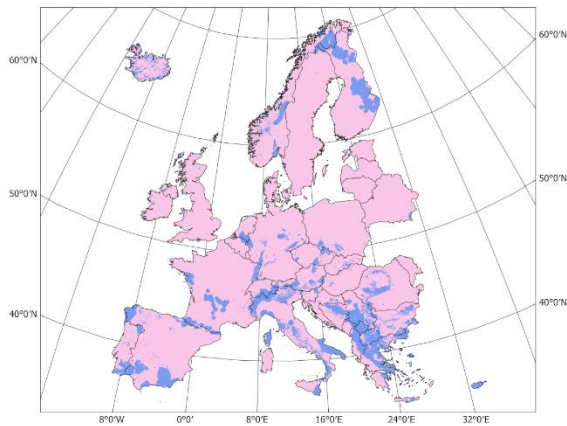
F. SER6 - Banded Iron Formations



G. SER7 - Rift-inversion Orogens



H. SER8 - Remaining Areas



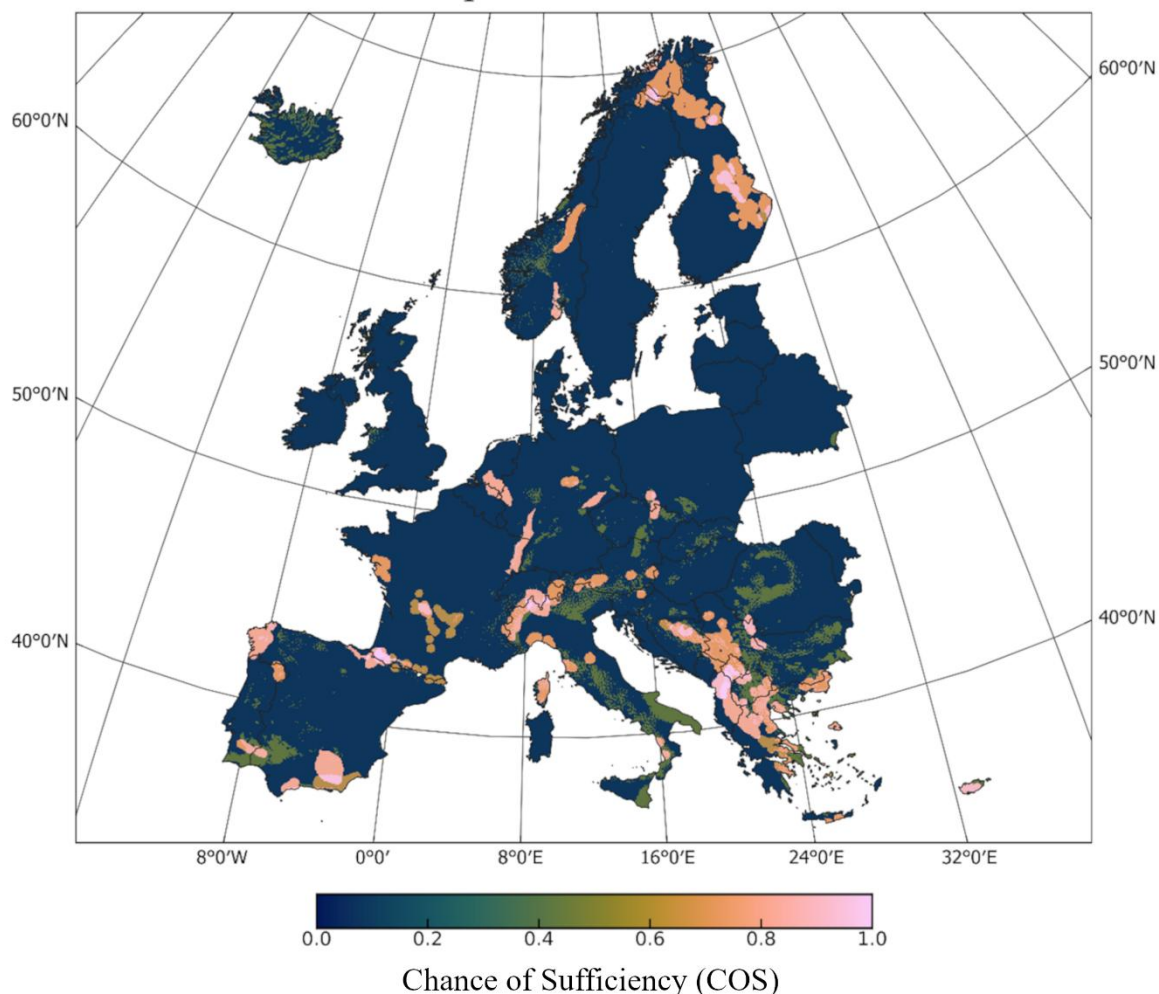
 Presence
 No presence

123

124 **Figure 2 |** Geological indicators included in the serpentinization (SER) source layer. **A–C:** Ultramafic bodies
125 with low (SER1), medium (SER2), and high (SER3) COS. **D:** Failed rift systems (SER4). **E:** Gravity anomalies
126 >40 mGal (SER5). **F:** Banded iron formations (SER6). **G:** Rift-inversion orogens (SER7). **H:** Remaining areas.

127 The serpentinization composite layer comprises eight sublayers (SER1–SER8), as shown in Figure
128 2. The first three layers (SER1–SER3) reflect the spatial distribution of ultramafic bodies with a 20
129 km buffer and COS weights based on depth classification. SER4 includes failed rift systems,
130 which can expose mantle rocks via crustal thinning and isostatic uplift (Gillard et al., 2019;
131 Gelman et al., 2025). SER5 represents positive gravity anomalies exceeding 40 mGal, which may
132 indicate dense ultramafic material in the subsurface (Escartin & Cannat, 1999; Bureau
133 Gravimétrique International, 2012). SER6 includes banded iron formations, capable of generating
134 hydrogen through low-temperature oxidation of ferrous iron (Geymond et al., 2022). SER7
135 identifies rift-inversion orogens—recently proposed as potential hydrogen-rich structures due to
136 mantle exhumation and favorable trapping conditions (Zwaan et al., 2025). SER8 encompasses
137 all other areas not covered by the previous sublayers and is assigned a uniform, low COS value
138 to account for unidentified sources. Figure 3 shows the resulting composite serpentinization
139 source layer, integrating SER1–SER8 using the COS values from Table 1.

Serpentinitization COS



140

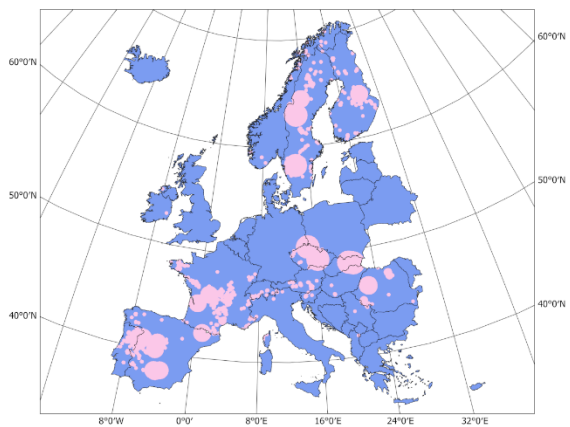
141 **Figure 3 | Composite COS map for serpentinitization sources, based on SER1–SER8.**

142 3.1.2 Radiolysis

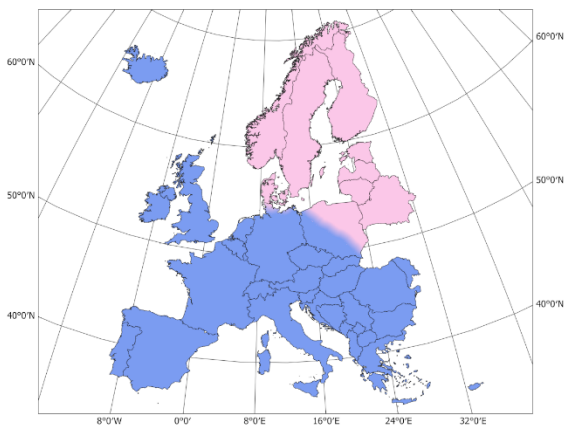
143 Radiolysis involves the dissociation of water molecules by ionizing radiation, forming reactive
144 species that recombine to produce molecular hydrogen. This process occurs in the presence of
145 radioactive materials such as uranium and thorium. Three geological indicators were included
146 (Figure 4): RAD1: Documented uranium occurrences across Europe, buffered according to
147 deposit size (EGDI, 2021). RAD2: The East European Craton—composed of stable, uranium-
148 enriched Precambrian basement rock (Asch, 2005; Lollar et al., 2014). RAD3: Accreted terranes,
149 representing geologically younger regions with variable radiogenic potential and less time for
150 hydrogen accumulation (Gelman et al., 2025). This layer serves as the inverse of RAD2.
151 Phanerozoic granitoids were excluded due to limited data coverage across Europe and their low
152 expected contribution. Figure 5 presents the composite COS map for radiolysis sources,
153 constructed from RAD1–RAD3 and corresponding COS values from Table 1.

154

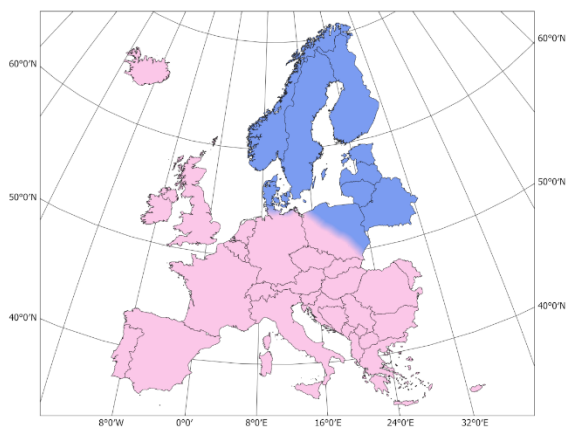
A. RAD1 - Uranium Occurrence



B. RAD2 - Precambrian Craton



C. RAD3 - Accreted Terranes

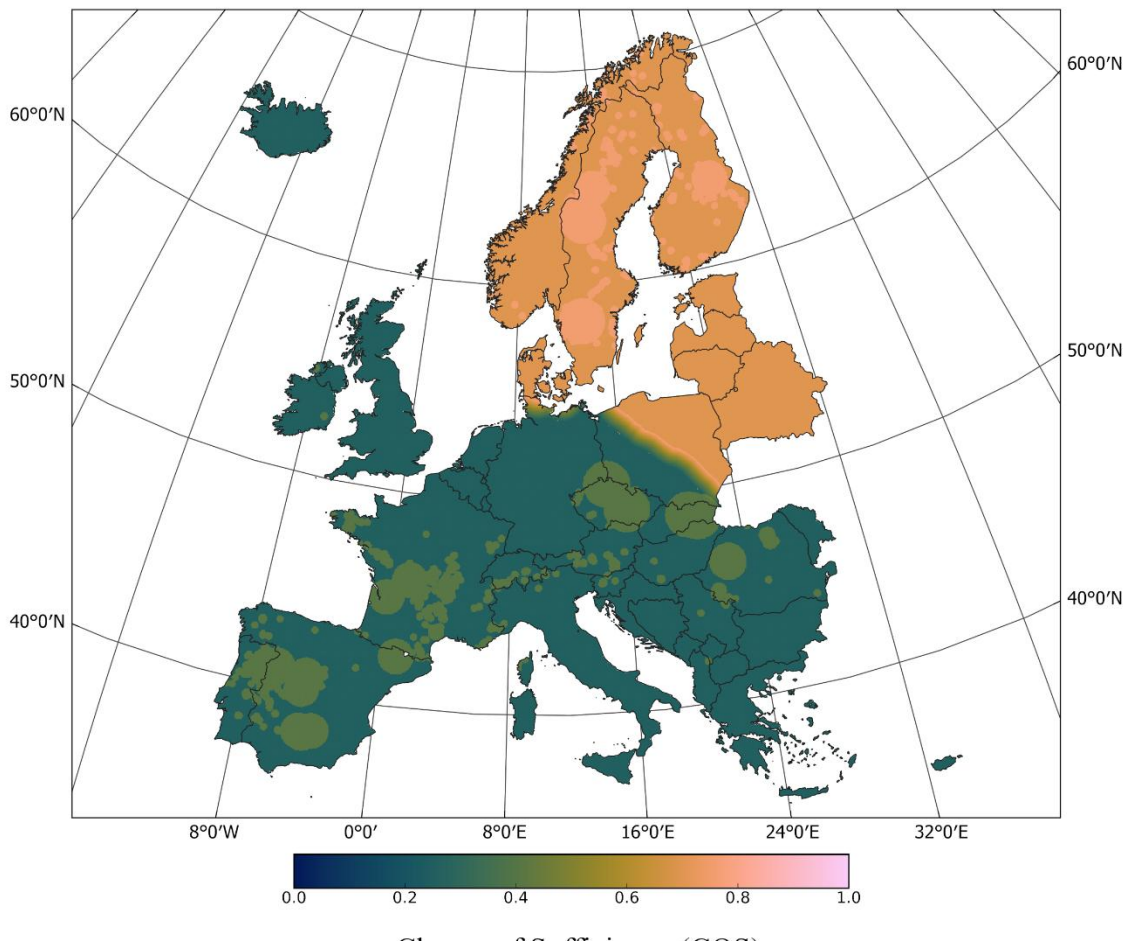


Presence
 No presence

155

156 **Figure 4 |** Geological indicators for radiolysis (RAD) source layer. **A:** Uranium occurrences (RAD1). **B:** East
157 European Craton with 100 km buffer (RAD2). **C:** Accreted terranes with 100 km buffer (RAD3).

Radiolysis COS



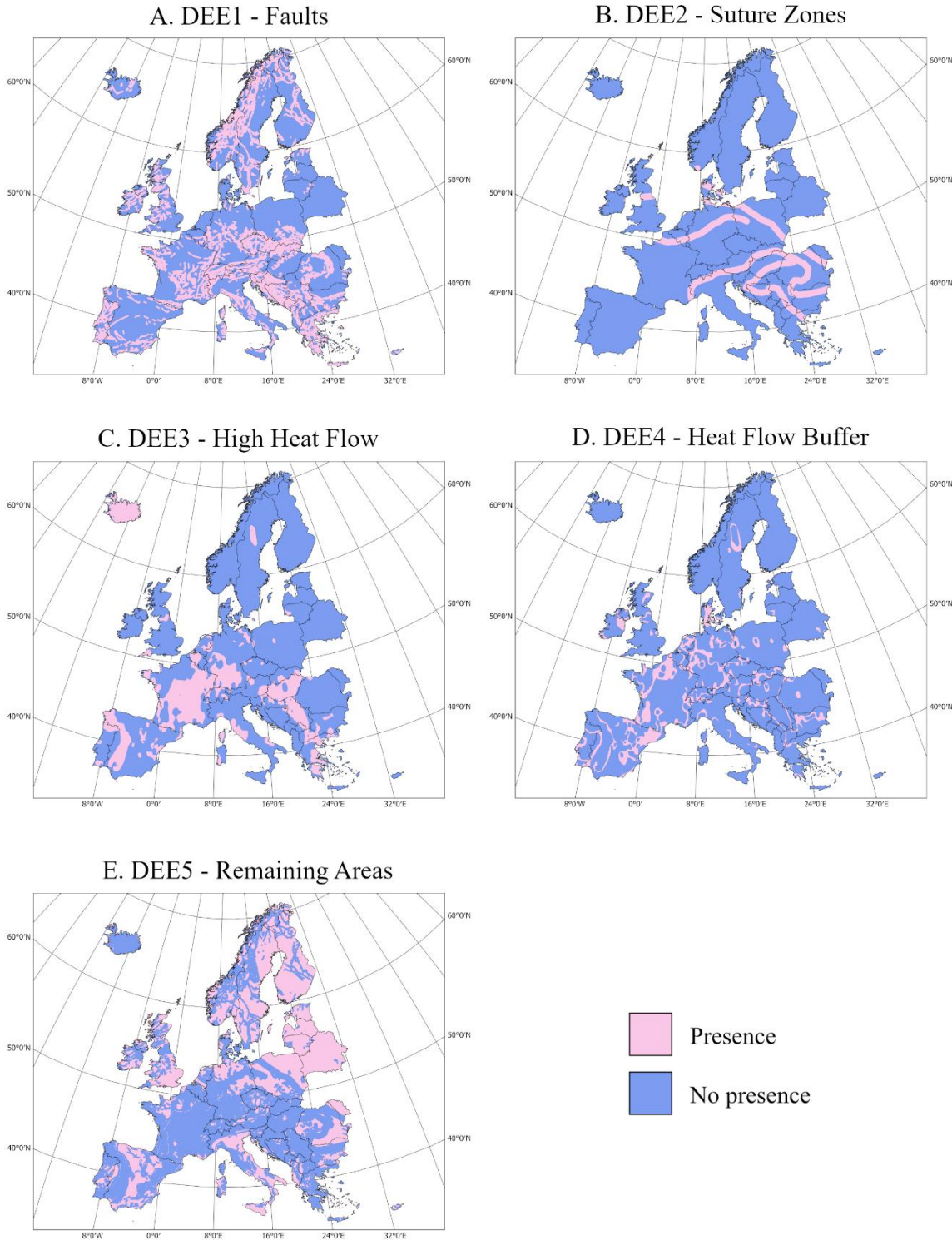
158

159 **Figure 5 |** Composite COS map for radiolysis sources based on layers RAD1–RAD3.

160 A clear spatial differentiation is observed between the East European Craton and the younger,
161 geologically complex regions of central and western Europe. High COS values dominate in
162 Scandinavia and the Baltic states, consistent with extensive, long-lived radiolytic environments.

163 3.1.3 Deep sources

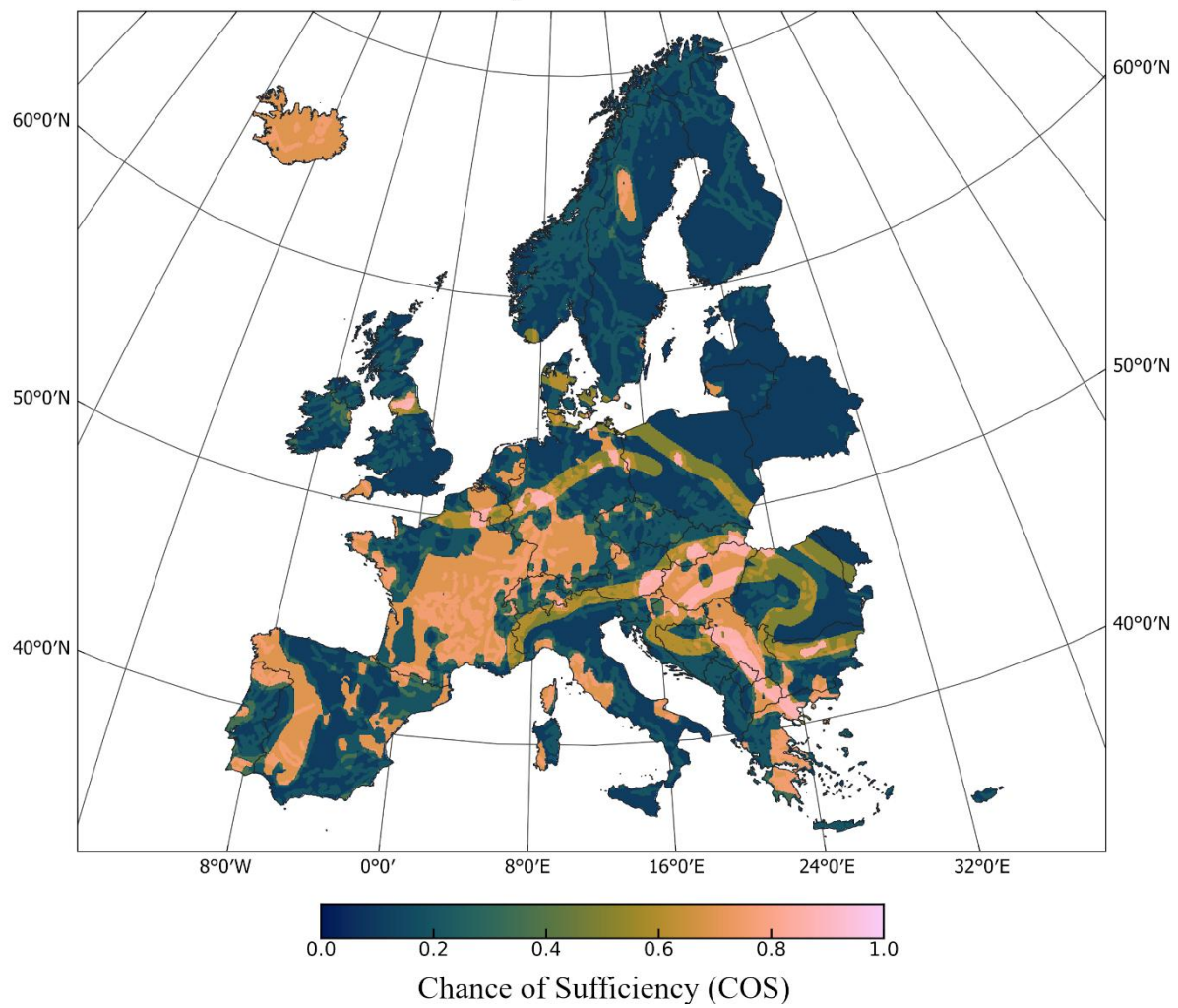
164 Hydrogen generated in the Earth's mantle via degassing or deep serpentinization may migrate
165 upward through the crust. The identification of migration pathways and thermal regimes is critical
166 in assessing this deep source potential. The deep source composite layer includes five indicators
167 (Figure 6): DEE1: Major fault systems with a 10 km buffer, representing conduits for upward gas
168 migration (Liu et al., 2023). DEE2: Suture zones—boundaries between tectonic terranes—which
169 are favorable for fluid transport (Lefevre et al., 2024). DEE3: Regions of elevated heat flow (>80
170 mW/m^2), associated with enhanced hydrothermal circulation and gas mobility (Chamorro et al.,
171 2013). DEE4: A transition buffer zone ($70\text{--}80 \text{ mW/m}^2$), assigned lower COS values. DEE5: Residual
172 areas not covered by the above features, with a minimal COS value assigned to account for
173 unknown sources. The composite deep source layer, shown in Figure 7, reflects increased
174 hydrogen prospectivity in regions with dense fault networks and elevated heat flow, particularly
175 in Iceland and parts of France.



176

177 **Figure 6 |** Geological indicators for deep source (DEE) potential. **A:** Faults with 10 km buffer
 178 (**DEE1**). **B:** Suture zones with 40 km buffer (**DEE2**). **C:** Heat flow >80 mW/m² (**DEE3**). **D:** Transition
 179 heat flow zone (70–80 mW/m², **DEE4**). **E:** Residual areas (**DEE5**).

Deep Source COS



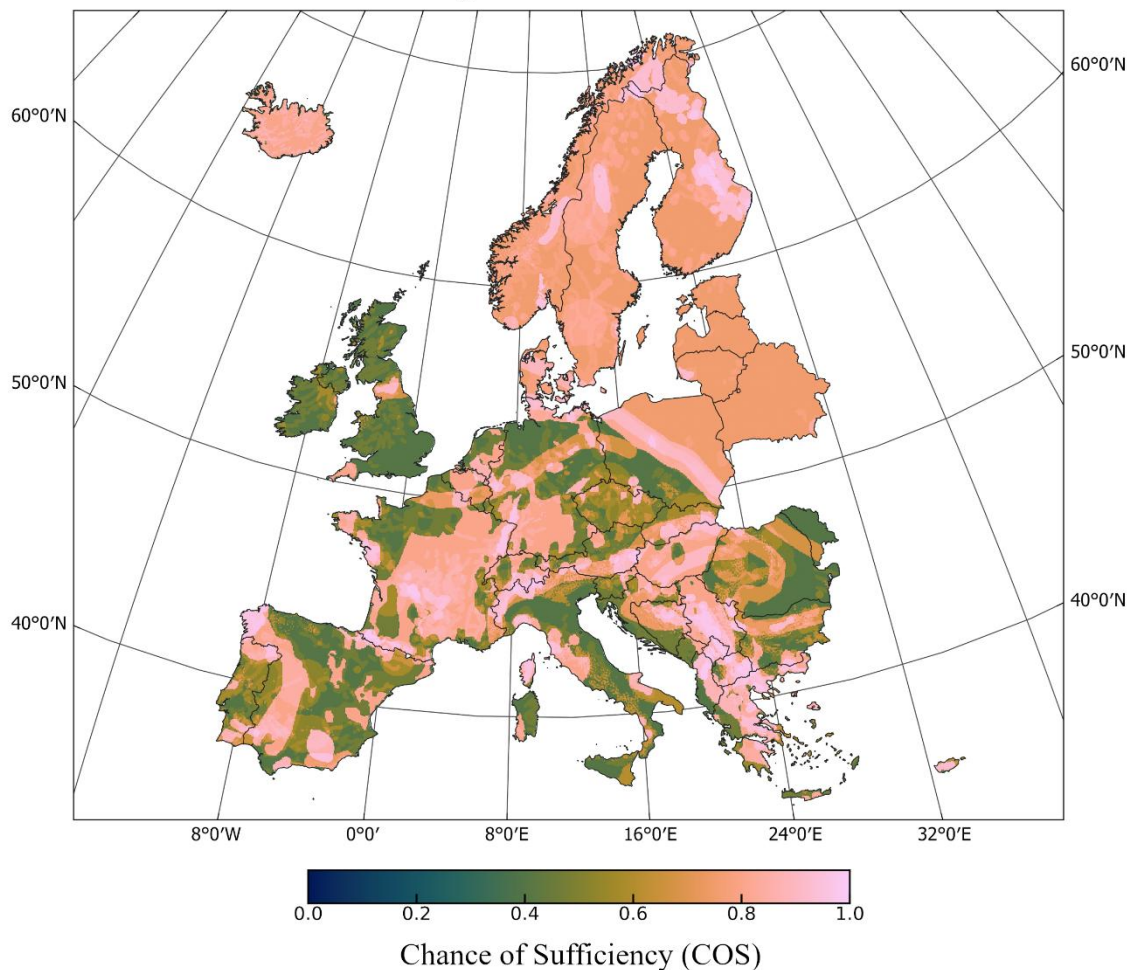
180

181 **Figure 7 | Composite COS map for deep source hydrogen potential, based on DEE1–DEE5.**

182 The three hydrogen source components—serpentinitization, radiolysis, and deep-source
183 processes—were integrated to produce a composite source map, shown in Figure 8. This layer
184 reflects the overall chance of sufficiency (COS) for hydrogen generation across Europe,
185 accounting for multiple geological processes and their respective indicators.

186 The influence of the East European Craton, a stable Precambrian geological unit, is clearly visible
187 in the composite map due to its high radiolytic potential. Additionally, several Balkan countries
188 display elevated COS values, highlighting regions with potentially favorable conditions for natural
189 hydrogen generation. However, it is important to note that hydrogen generation alone is
190 insufficient to define prospectivity. The viability of these regions depends on the presence of
191 adequate reservoir and seal formations, which are addressed in the following section.

Composite Source COS



192

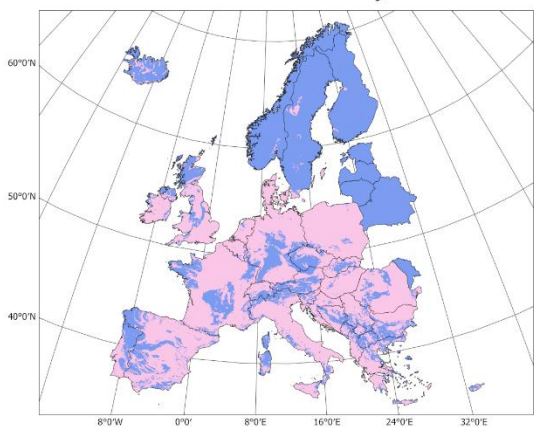
193 **Figure 8 | Composite COS map for hydrogen source potential, combining the serpentinization,**

194 radiolysis, and deep-source subcomponents.

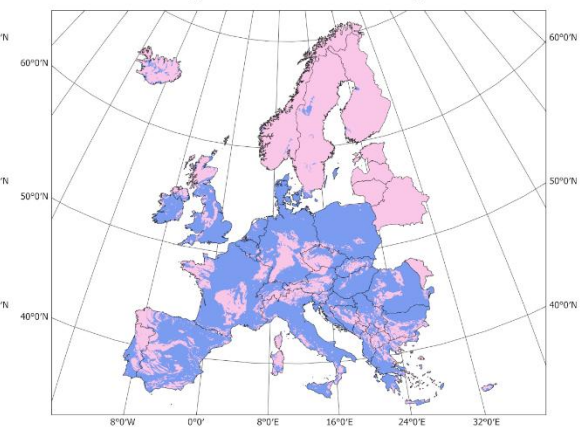
195 3.2 Potential reservoirs

196 For hydrogen to accumulate in economically viable quantities and contribute meaningfully to the
197 energy transition, the presence of a porous and permeable reservoir is essential. Accordingly,
198 sedimentary rocks, which typically exhibit such characteristics, are given higher COS values and
199 are mapped in layer RES1 (Asch, 2005; Maiga, 2023). In contrast, layer RES2 represents igneous
200 and metamorphic rocks, which generally exhibit lower porosity and are assigned lower COS
201 values. Additionally, layer RES3 maps the extent of sedimentary basins, which are considered
202 favourable due to their thick accumulations of sedimentary sequences that may host large-scale
203 reservoirs (Gelman et al., 2025). These three reservoir-related indicators are shown in Figure 9,
204 and their integration results in the composite reservoir COS map, displayed in Figure 10.

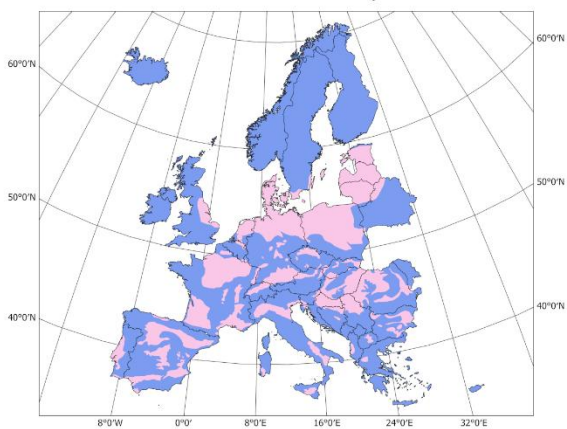
A. RES1 - Sedimentary Rocks



B. RES2 - Igneous / Metamorphic Rocks



C. RES3 - Sedimentary Basins

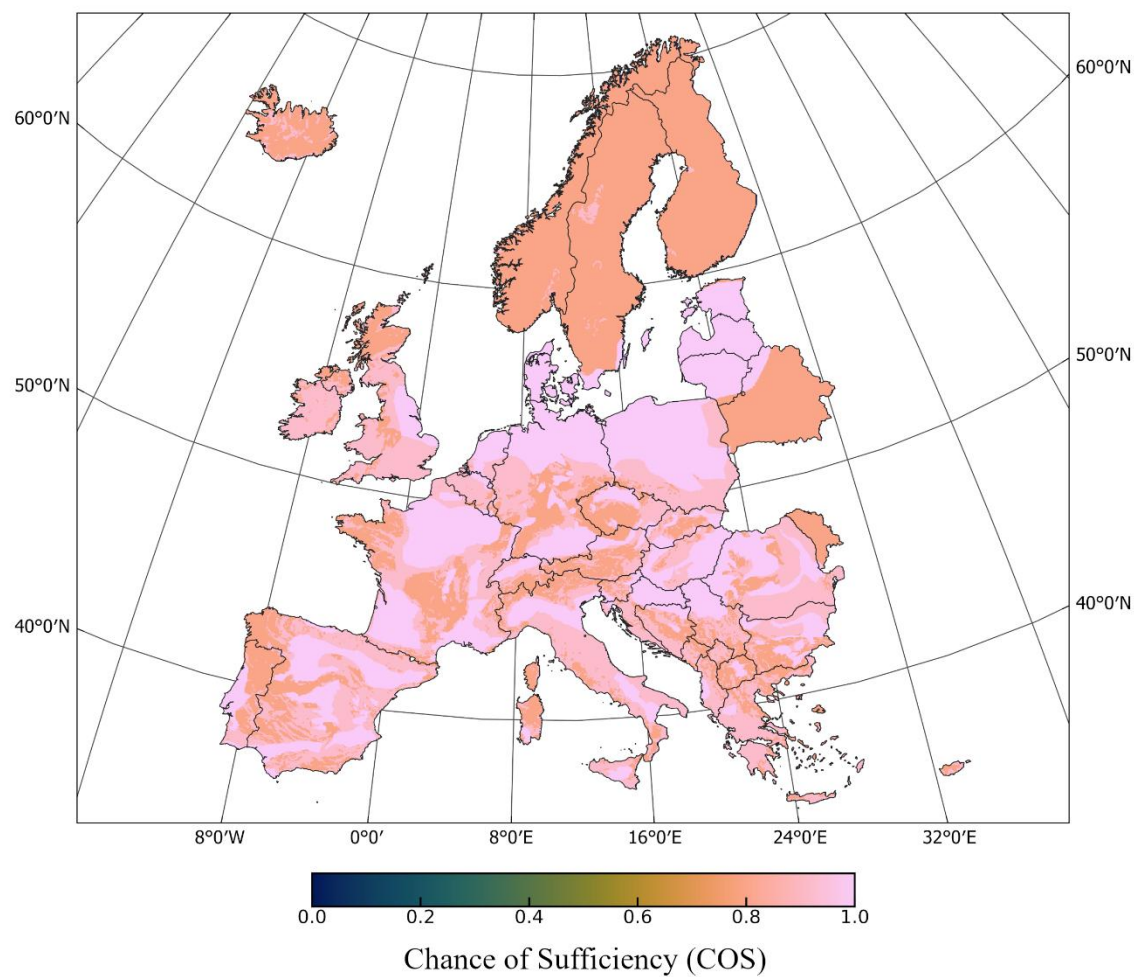


[Legend:
■ Presence
■ No presence]

205

206 **Figure 9 | Geological indicators used for reservoir assessment (RES).** A: Sedimentary rocks
207 (RES1); B: Igneous/metamorphic rocks (RES2); C: Sedimentary basins (RES3). Data sources are
208 listed in Table A.2 (Supplementary Materia).

Reservoir COS



209

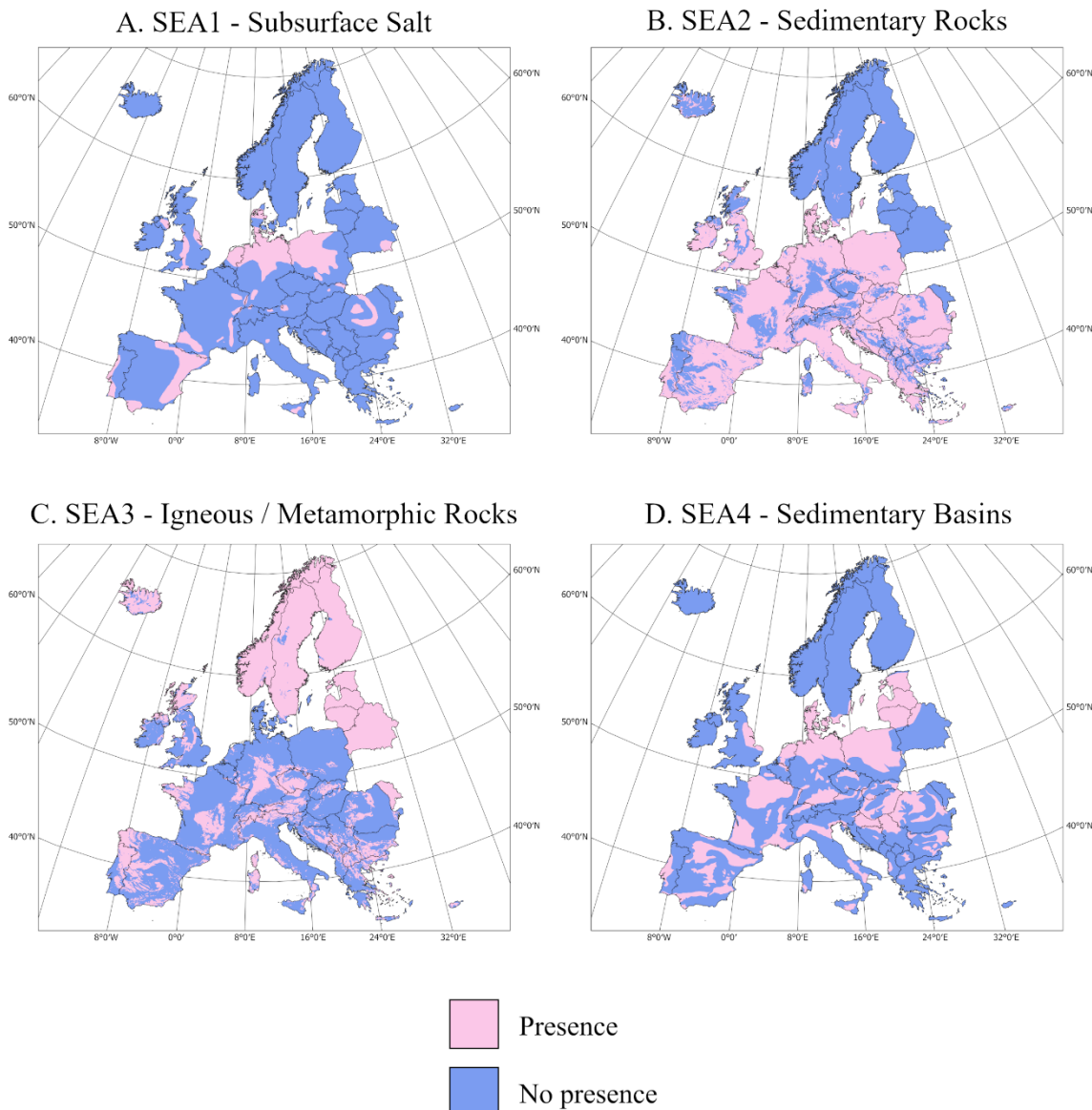
210 **Figure 10 | Composite COS map for reservoir suitability, based on layers RES1–RES3 and the**
211 **COS values in Table 1.**

212

213

214 3.3 Seals

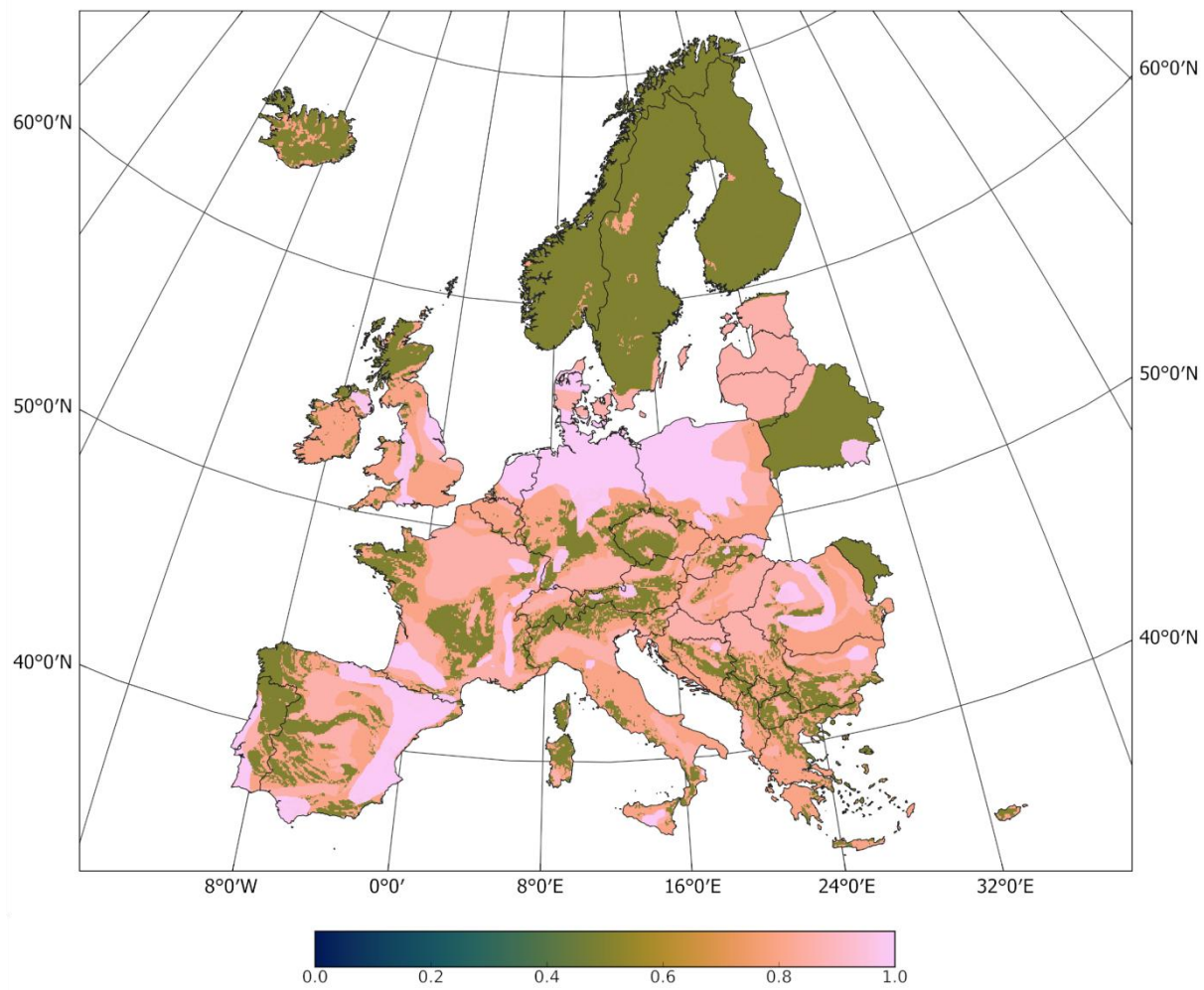
215 Effective hydrogen accumulation also requires a subsurface seal to prevent upward migration
 216 and escape to the atmosphere. The most effective of these are salt layers, mapped as SEA1, due
 217 to their extremely low permeability and proven sealing capabilities (Beauheim & Roberts, 2002).
 218 In addition, SEA2–SEA4 mirror the lithologies and structures used in the reservoir analysis (RES1–
 219 RES3), but with COS values adjusted to reflect their sealing potential (Gelman et al., 2025).
 220 Sedimentary rocks and basins, in particular, may contain interbedded shale or evaporite layers
 221 that can act as effective seals. These indicators are shown in Figure 11, and their integration
 222 yields the composite seal layer shown in Figure 12.



223

224 **Figure 11 | Geological indicators used for seal assessment (SEA).** **A:** Subsurface salt (SEA1); **B:** Sedimentary
 225 rocks (SEA2); **C:** Igneous/metamorphic rocks (SEA3); **D:** Sedimentary basins (SEA4). Data sources are
 226 listed in Table A.2 (Supplementary Material).

Seal COS



227

Chance of Sufficiency (COS)

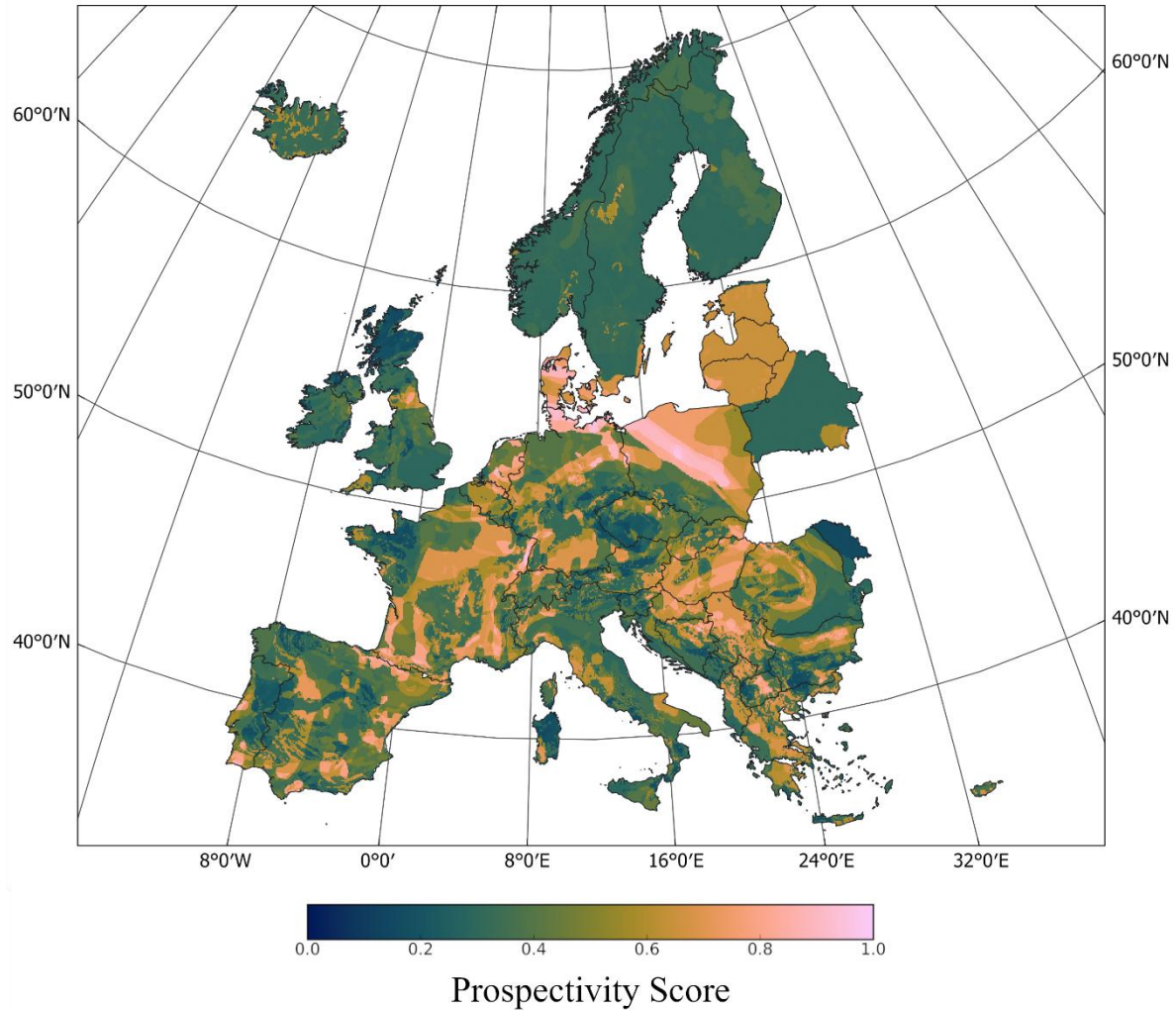
228 **Figure 12 | Composite COS map for seal potential, based on layers SEA1–SEA4 and COS values in Table 1.**

229 3.4 Prospectivity of natural hydrogen

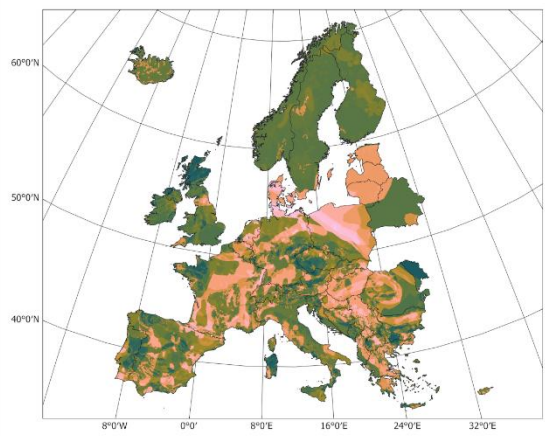
230 The final prospectivity map (Figure 13) is produced by integrating the composite source, reservoir,
231 and seal layers. This map represents the overall chance of sufficiency (COS) for hydrogen
232 prospectivity across Europe, reflecting regions where hydrogen generation potential coincides
233 with suitable trapping and storage conditions.

234 The highest prospectivity scores are identified in Poland, Denmark, Hungary, and Serbia. Other
235 countries, including France and Germany, show moderate to high potential in localized regions.
236 Notably, while Scandinavia exhibits a high source potential—primarily driven by radiolysis within
237 the Precambrian craton—its overall prospectivity is moderated by lower COS values for reservoir
238 and seal suitability.

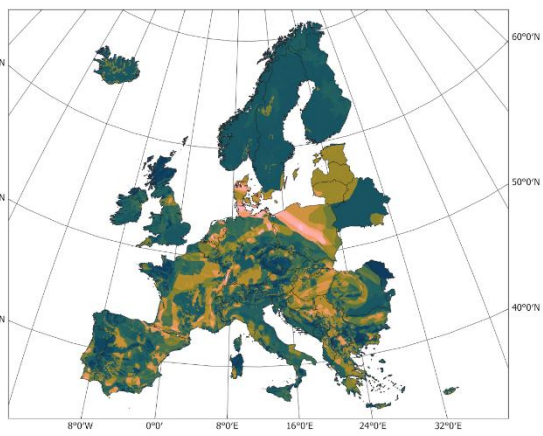
A. Hydrogen Prospectivity (P50)



B. P10 Prospectivity



C. P90 Prospectivity



239

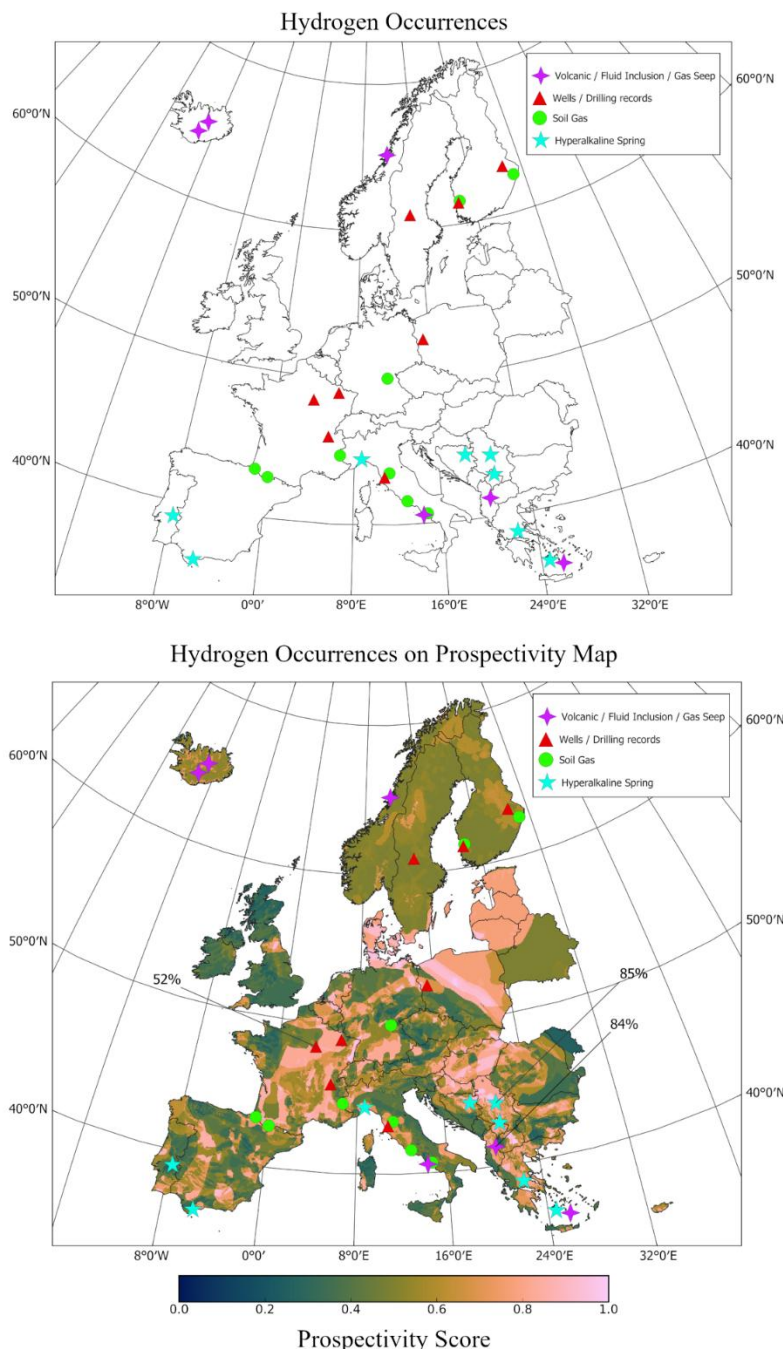
240 **Figure 13 |** Final natural hydrogen prospectivity map, derived by integrating the composite
241 source, reservoir, and seal layers using the methodology described in Section 2.

242

243

244 *3.5 Validation against known hydrogen occurrences*

245 To evaluate the reliability of the prospectivity model, the final map was compared with known
246 natural hydrogen occurrences compiled from the literature (Table A.3). These occurrences are
247 displayed in Figure 14, overlaid on the prospectivity map. For each documented occurrence, the
248 maximum local prospectivity score (as derived from the P50 map in Figure 13) was extracted and
249 recorded in Table A.3. The degree of spatial correlation between known hydrogen sites and
250 regions of high predicted prospectivity provides qualitative support for the model's validity.



251

252 **Figure 14 | Comparison of known hydrogen occurrences (icons) with the final prospectivity map.**
253 Occurrence data sources are listed in Table A.3 (Supplementary Material). The lower panel
254 overlays occurrences on the COS map shown in Figure 13.

255 A substantial number of documented natural hydrogen occurrences coincide with regions of high
256 predicted prospectivity, particularly in Italy, the Balkans (e.g., Serbia, Albania), and Greece.
257 Although Scandinavia displays a moderate overall prospectivity, the known occurrences there
258 align with localized areas of elevated COS values. Conversely, some high-prospectivity regions—
259 such as Denmark and Hungary—currently lack confirmed hydrogen occurrences, underscoring
260 their potential as priority targets for future exploration and validation efforts.

261 **4. Discussion**

262 This study presents the first continent-scale natural hydrogen prospectivity map for Europe,
263 integrating geological indicators of hydrogen generation, accumulation, and sealing. The map
264 aligns well with recently documented occurrences of natural hydrogen, such as in Albania (Lévy
265 et al., 2023), lending credibility to the methodology and underlying assumptions. By offering
266 geological context for these occurrences, the results not only help explain observed hydrogen
267 emissions but also highlight regions where generation potential coincides with viable reservoirs
268 and seals.

269 Regions with the highest predicted prospectivity include Denmark, Hungary, France, Poland,
270 North Macedonia, and Serbia. For some of these areas, hydrogen potential has already been
271 recognized. For example, the Lorraine region of France was recently targeted in a 2024 exploration
272 campaign (Meillaud & King, 2023; Waltham, 2024), and assessments are ongoing in Denmark
273 (Geocenter Denmark, 2025). In contrast, other promising regions such as Hungary have received
274 little to no attention in this context. The abundance of deep hydrogen source indicators and
275 potential reservoir structures in Hungary suggest it should be prioritized in future field
276 investigations.

277 Conversely, areas like Norway, Sweden, and Finland—despite exhibiting strong indicators for
278 hydrogen generation (particularly radiolysis)—show moderate to low overall prospectivity. This is
279 primarily due to the limited presence of sedimentary reservoirs and sealing formations across the
280 Fennoscandian Shield, where crystalline basement rocks dominate (Rosberg & Erlström, 2021).
281 This contrasts with findings from North America, where radiolytic hydrogen in cratonic settings is
282 considered more viable due to the presence of thick sedimentary cover (Marshak & van der
283 Pluijm, 2020; Gelman et al., 2025). Nevertheless, recent research suggests that in-situ hydrogen
284 generation via geological stimulation of ultramafic rocks may offer a path forward even in shield
285 regions (Templeton et al., 2024). The compilation of ultramafic bodies provided in this study
286 (Supplementary Material A.1) can therefore serve not only for passive exploration but also as a
287 guide for potential stimulation-based approaches.

288 This study is subject to several limitations. First, offshore areas were excluded, despite their
289 significant potential. For instance, the failed rift basins beneath the North Sea—characterized by
290 thick sedimentary sequences and abundant salt structures—may present ideal conditions for
291 hydrogen generation, migration, and trapping (Rattey & Hayward, 1999). Second, hydrogen
292 migration processes were not explicitly modelled. Subsurface migration is critical for

293 understanding accumulation potential, especially in faulted or rifted terrains. Previous studies
294 have successfully applied hydrocarbon-based flow path models to hydrogen (Gelman et al.,
295 2025), and numerical simulations have demonstrated fault-facilitated hydrogen transport (Donzé
296 et al., 2022). Integrating such migration models with offshore data would provide a more
297 complete prospectivity assessment.

298 Advancements in remote sensing and machine learning also offer promising avenues for
299 improving exploration efficiency. Algorithms trained on surface expressions of hydrogen (e.g.,
300 vegetation anomalies, gas seepage signatures) could help refine subsurface targeting in high-
301 COS regions identified in this study (Ohio State University, 2023).

302 Finally, this analysis relied on Europe-wide datasets, which, while suitable for a first-order
303 screening study, vary in quality and resolution. These compilations often reflect heterogeneous
304 national datasets with differing classification standards, completeness, and scale. As such,
305 detailed national-scale analyses in high-prospectivity countries—particularly those currently
306 underexplored—are essential next steps. Expanding and standardizing datasets on key
307 parameters, such as subsurface uranium distribution, would greatly enhance the resolution and
308 reliability of future continent-wide assessments.

309 **5. Conclusions**

310 This study presents the first continent-scale prospectivity assessment for natural hydrogen in
311 Europe, offering a foundational spatial framework for early-stage exploration. By integrating
312 indicators of hydrogen generation—through serpentinization, radiolysis, and deep-sourced
313 processes—with assessments of potential reservoirs and sealing formations, a comprehensive
314 map of relative hydrogen prospectivity was developed.

315 A novel element of this work is the systematic compilation of ultramafic rock bodies across
316 Europe, serving as a critical input for evaluating serpentinization potential. The integration of
317 multiple geological datasets and Monte Carlo-based uncertainty modelling enabled the
318 identification of several high-prospectivity regions, most notably in Hungary, Denmark, Poland,
319 Serbia, and parts of France and North Macedonia. These results are consistent with many known
320 hydrogen occurrences and also highlight underexplored regions where field validation and further
321 research are urgently warranted.

322 While the study focuses on onshore areas and does not incorporate dynamic hydrogen migration
323 models, it provides a crucial first-order screening tool. The methodology and datasets developed
324 here can be used as a basis for more detailed national assessments and support future
325 incorporation of offshore data, geochemical modelling, and migration pathway simulations.

326 In the context of the energy transition, natural hydrogen represents a potentially low-cost,
327 carbon-free energy source. Its viability will ultimately depend on resource accessibility,
328 renewability, regulatory frameworks, and technological developments in detection, stimulation,
329 and extraction. By identifying regions where favourable geological conditions overlap, this study
330 supports strategic exploration planning and emphasizes Europe's potential to harness natural
331 hydrogen as part of a broader transition toward sustainable and secure energy systems.

332

333 **CRediT statement**

334 **FHJW:** Methodology, software, formal analysis, investigation, visualisation, writing original draft.

335 **JMM:** Conceptualisation, supervision, writing – review & editing.

336

337 **References**

338 Aertgeerts, G. (2016). Étude pétrologique des reliques ophiolitiques des complexes de Champtoceaux et
339 d'Audierne : caractérisation des minéraux fibreux dans les roches mafiques et ultramafiques.

340 <http://hal.univ-nantes.fr/tel-01286275v1>

341 Aimar, L., Frery, E., Strand, J., Heath, C., Khan, S., Moretti, I., & Ong, C. (2023). Natural hydrogen seeps or
342 salt lakes: how to make a difference? Grass Patch example, Western Australia. *Frontiers in Earth Science*,
343 11. <https://doi.org/10.3389/feart.2023.1236673>

344 Allard, P., Maiorani, A., Tedesco, D., Cortecchi, G., & Turi, B. (1991). Isotopic study of the origin of sulfur and
345 carbon in Solfatara fumaroles, Campi Flegrei caldera. *Journal of Volcanology and Geothermal Research*,
346 48(1–2), 139–159. [https://doi.org/10.1016/0377-0273\(91\)90039-3](https://doi.org/10.1016/0377-0273(91)90039-3)

347 Asch, K. (2005). International Geological Map of Europe and Adjacent Areas 1 : 5 000 000 (IGME5000)
348 [Geological map]. Bundesanstalt für Geowissenschaften und Rohstoffe; Commission for the Geological
349 Map of the World. <https://doi.org/10.25928/igme-5000>

350 Balen, D., & Massonne, H. (2021). Two contrasting P-T paths for metamorphic sole amphibolites of the
351 Dinaride Ophiolite Zone (Krivaja-Konjuh ultramafic massif, Central Bosnia and Herzegovina) and their
352 geodynamic implications. *Lithos*, 394–395, 106184. <https://doi.org/10.1016/j.lithos.2021.106184>

353 Ballentine, C.J., Karolytė, R., Cheng, A. et al. Natural hydrogen resource accumulation in the continental
354 crust. *Nat Rev Earth Environ* 6, 342–356 (2025). <https://doi.org/10.1038/s43017-025-00670-1>

355 Bazylev, B. A., Karamata, S., & Zakariadze, G. S. (2003). Petrology and evolution of the Brezovica
356 ultramafic massif, Serbia. *Geological Society London Special Publications*, 218(1), 91–108.
357 <https://doi.org/10.1144/gsl.sp.2003.218.01.06>

358 Beqiraj, A. (2000). Geochemical Characterization of Podiform Chromite Ores from the Ultramafic Massif
359 of Bulqiza (Eastern Ophiolitic Belt, Albania) and Hints for Exploration. *Exploration and Mining Geology*,
360 9(2), 149–156. <https://doi.org/10.2113/0090149>

361 Berger, J., Femenias, O., Mercier, J. C. C., & Demaiffe, D. (2005). Ocean-floor hydrothermal
362 metamorphism in the Limousin ophiolites (western French Massif Central): evidence of a rare preserved
363 Variscan oceanic marker. *Journal of Metamorphic Geology*, 23(9), 795–812.
364 <https://doi.org/10.1111/j.1525-1314.2005.00610.x>

365 Bermejo, R. M. B., Ramírez, P. B., De Balbín Behrmann, R., & De Los Ángeles Lancharro Gutiérrez, M.
366 (2017). Production and consumption of salt in the inland Tagus Valley in Prehistory (Spain). *KEY
367 RESOURCES AND SOCIO-CULTURAL DEVELOPMENTS IN THE IBERIAN CHALCOLITHIC*, 89–105.
368 <https://dx.doi.org/10.15496/publikation-19737>

369 Bicocchi, G., Tassi, F., Bonini, M., Capecchiacci, F., Ruggieri, G., Buccianti, A., Burgassi, P., & Vaselli, O.
370 (2013). The high pCO₂ Caprese Reservoir (Northern Apennines, Italy): Relationships between present-
371 and paleo-fluid geochemistry and structural setting. *Chemical Geology*, 351, 40–56.
372 <https://doi.org/10.1016/j.chemgeo.2013.05.001>

- 373 Blanco, H., & Faaij, A. (2017). A review at the role of storage in energy systems with a focus on Power to
374 Gas and long-term storage. *Renewable and Sustainable Energy Reviews*, 81, 1049–1086.
375 <https://doi.org/10.1016/j.rser.2017.07.062>
- 376 Boev, B., Cvetković, V., Prelević, D., Šarić, K., & Boev, I. (2018). EAST VARDAR OPHIOLITES REVISITED: A
377 BRIEF SYNTHESIS OF GEOLOGY AND GEOCHEMICAL DATA. *Contributions Section of Natural*
378 *Mathematical and Biotechnical Sciences*, 39(1), 51.
379 <https://doi.org/10.20903/csnmbs.masa.2018.39.1.119>
- 380 Bogatu, A., Giselle, S., Tremblay, A., Meshi, A., & Bédard, J. (2019). Western- and Eastern-type ultramafic
381 massifs of the Mirdita ophiolite, Albania: structural evidence for lower-plate (Western-type) - upper-plate
382 (Eastern-type) relationships and formation of a Jurassic oceanic core complex. *EGUGA*, 11952.
383 <http://ui.adsabs.harvard.edu/abs/2019EGUGA..2111952B/abstract>
- 384 Bonnemains, D., Carlut, J., Escartín, J., Mével, C., Andreani, M., & Debret, B. (2016). Magnetic signatures
385 of serpentinitization at ophiolite complexes. *Geochemistry Geophysics Geosystems*, 17(8), 2969–2986.
386 <https://doi.org/10.1002/2016gc006321>
- 387 Bonvalot, S., Briais, A., Kuhn, M., Peyrefitte, A., Vales, N., Biancale, R., Gabalda, G., Moreaux, G.,
388 Reinquin, F. & Sarrailh, M. (2012). Global grids : World Gravity Map (WGM2012). Bureau Gravimetrique
389 International. <https://doi.org/10.18168/bgi.23>
- 390 Brunet, F., Malvoisin, B. (2025). Can natural H₂ be considered renewable? The reference case of a deep
391 aquifer in an intracratonic sedimentary basin. *Advances in Geochemistry and Cosmochemistry* 1(2), 738-
392 738. <https://doi.org/10.33063/agc.v1i2.738>
- 393 Byrd Polar & Climate Research Center. (2023, December 30). AI mapping reveals potential subsurface
394 natural hydrogen worldwide. The Ohio State University. Retrieved June 14, 2025, from
395 <https://byrd.osu.edu/news/ai-mapping-reveals-potential-subsurface-natural-hydrogen-worldwide>
- 396 Caglayan, D. G., Weber, N., Heinrichs, H. U., Linßen, J., Robinius, M., Kukla, P. A., & Stolten, D. (2020).
397 Technical potential of salt caverns for hydrogen storage in Europe. *International Journal of Hydrogen
398 Energy*, 45(11), 6793–6805. <https://doi.org/10.1016/j.ijhydene.2019.12.161>
- 399 Campbell, S. D. G., Howells, M. F., Smith, M., & Reedman, A. J. (1988). A Caradoc Failed-Rift within the
400 Ordovician Marginal Basin of Wales. *Geological Magazine*, 125(3), 257–266.
401 <https://doi.org/10.1017/s0016756800010190>
- 402 Canérot, J. (2017). The pull apart-type Tardets-Mauléon Basin, a key to understand the formation of the
403 Pyrenees. *BSGF – Earth Sciences Bulletin*, 188(6), 35. <https://doi.org/10.1051/bsgf/2017198>
- 404 Carapezza, M. L., & Tarchini, L. (2007). Accidental gas emission from shallow pressurized aquifers at
405 Alban Hills volcano (Rome, Italy): Geochemical evidence of magmatic degassing? *Journal of Volcanology
406 and Geothermal Research*, 165(1–2), 5–16. <https://doi.org/10.1016/j.jvolgeores.2007.04.008>
- 407 CGS Europe. (2013). Pan-European coordination action on CO₂ geological storage. European
408 Commission. Retrieved from <https://cordis.europa.eu/project/id/256725>
- 409 Chamorro, C. R., García-Cuesta, J. L., Mondéjar, M. E., & Pérez-Madrazo, A. (2013). Enhanced geothermal
410 systems in Europe: An estimation and comparison of the technical and sustainable potentials. *Energy*,
411 65, 250–263. <https://doi.org/10.1016/j.energy.2013.11.078>
- 412 Chavagnac, V., Ceuleneer, G., Monnin, C., Lansac, B., Hoareau, G., & Boulart, C. (2013). Mineralogical
413 assemblages forming at hyperalkaline warm springs hosted on ultramafic rocks: A case study of Oman

- 414 and Ligurian ophiolites. *Geochemistry Geophysics Geosystems*, 14(7), 2474–2495.
415 <https://doi.org/10.1002/ggge.20146>
- 416 Chiodini, G., Frondini, F., Cardellini, C., Granieri, D., Marini, L., & Ventura, G. (2001). CO₂ degassing and
417 energy release at Solfatara volcano, Campi Flegrei, Italy. *Journal of Geophysical Research Atmospheres*,
418 106(B8), 16213–16221. <https://doi.org/10.1029/2001jb000246>
- 419 Cloetingh, S., & Cornu, T. (2005). Neotectonics and Quaternary fault-reactivation in Europe's intraplate
420 lithosphere. Elsevier. <https://research.vu.nl/en/publications/neotectonics-and-quaternary-fault->
421 [reactivation-in-europes-intrapl](https://research.vu.nl/en/publications/neotectonics-and-quaternary-fault-reactivation-in-europes-intrapl)
- 422 Collins, L. (2023, May 16). “Significant concentrations” of natural hydrogen discovered in northeast
423 France by local power and gas producer. hydrogeninsight.com.
424 <https://www.hydrogeninsight.com/production/significant-concentrations-of-natural-hydrogen->
425 [discovered-in-northeast-france-by-local-power-and-gas-producer/2-1-1452270](https://www.hydrogeninsight.com/production/significant-concentrations-of-natural-hydrogen-discovered-in-northeast-france-by-local-power-and-gas-producer/2-1-1452270)
- 426 Combaudon, V., Moretti, I., Kleine, B. I., & Stefánsson, A. (2022). Hydrogen emissions from hydrothermal
427 fields in Iceland and comparison with the Mid-Atlantic Ridge. *International Journal of Hydrogen Energy*,
428 47(18), 10217–10227. <https://doi.org/10.1016/j.ijhydene.2022.01.101>
- 429 Criss, R. E. (2019). Thermal models of the continental lithosphere. In Elsevier eBooks (pp. 151–174).
430 <https://doi.org/10.1016/b978-0-12-818430-1.00006-9>
- 431 Daae, F. L., Økland, I., Dahle, H., Jørgensen, S. L., Thorseth, I. H., & Pedersen, R. B. (2013). Microbial life
432 associated with low-temperature alteration of ultramafic rocks in the Leka ophiolite complex. *Geobiology*,
433 11(4), 318–339. <https://doi.org/10.1111/gbi.12035>
- 434 Daskalopoulou, K., Gagliano, A. L., Calabrese, S., Longo, M., Hantzis, K., Kyriakopoulos, K., &
435 D'Alessandro, W. (2018). Gas geochemistry and CO₂ output estimation at the island of Milos, Greece.
436 *Journal of Volcanology and Geothermal Research*, 365, 13–22.
437 <https://doi.org/10.1016/j.jvolgeores.2018.10.003>
- 438 De Hoog, J. C., Janák, M., Vrabec, M., & Froitzheim, N. (2008). Serpentinitised peridotites from an ultrahigh-
439 pressure terrane in the Pohorje Mts. (Eastern Alps, Slovenia): Geochemical constraints on petrogenesis
440 and tectonic setting. *Lithos*, 109(3–4), 209–222. <https://doi.org/10.1016/j.lithos.2008.05.006>
- 441 Deronzier, J., & Giouse, H. (2020). Vaux-en-Bugey (Ain, France): the first gas field produced in France,
442 providing learning lessons for natural hydrogen in the sub-surface? *BSGF – Earth Sciences Bulletin*, 191,
443 7. <https://doi.org/10.1051/bsgf/2020005>
- 444 Deville, E., & Prinzhofer, A. (2016). The origin of N₂-H₂-CH₄-rich natural gas seepages in ophiolitic
445 context: A major and noble gases study of fluid seepages in New Caledonia. *Chemical Geology*, 440, 139–
446 147. <https://doi.org/10.1016/j.chemgeo.2016.06.011>
- 447 Donzé, F., Bourdet, L., Truche, L., Taillefer, A., Dutoit, H., Dusseaux, C., & Lefèuvre, N. (2022). Numerical
448 modeling of natural hydrogen migration from deep sources within fault zones. *Goldschmidt Abstracts*.
449 <https://doi.org/10.46427/gold2022.10924>
- 450 Donzé, F., Lefèuvre, N., Truche, L., Yao, Y., Vujević, I., & Dutoit, H. (2024). Natural hydrogen exploration
451 within western European and eastern Mediterranean ophiolites and ultramafic complexes. *Geochemistry*
452 *Exploration Environment Analysis*. <https://doi.org/10.1144/geochem2024-043>
- 453 Dugamin E., Truche L., Donzé F.V. (2019). Natural Hydrogen Exploration Guide, Geonum Ed.: ISRN
454 GEONUM-NST--2019-01--ENG, 16 pages.

- 455 Dèzes, P., Schmid, S., & Ziegler, P. (2004). Evolution of the European Cenozoic Rift System: interaction of
456 the Alpine and Pyrenean orogens with their foreland lithosphere. *Tectonophysics*, 389(1–2), 1–33.
457 <https://doi.org/10.1016/j.tecto.2004.06.011>
- 458 Ellis, G. S., & Gelman, S. E. (2024). Model predictions of global geologic hydrogen resources. *Science*
459 *Advances*, 10(50). <https://doi.org/10.1126/sciadv.ado0955>
- 460 Escartín, J., & Cannat, M. (1999). Ultramafic exposures and the gravity signature of the lithosphere near
461 the Fifteen-Twenty Fracture Zone (Mid-Atlantic Ridge, 14°–16.5°N). *Earth and Planetary Science Letters*,
462 171(3), 411–424. [https://doi.org/10.1016/s0012-821x\(99\)00169-7](https://doi.org/10.1016/s0012-821x(99)00169-7)
- 463 Etiope, G. (2024). Natural hydrogen extracted from ophiolitic rocks: A first dataset. *International Journal of*
464 *Hydrogen Energy*, 78, 368–372. <https://doi.org/10.1016/j.ijhydene.2024.06.292>
- 465 Etiope, G., Samardžić, N., Grassa, F., Hrvatović, H., Miošić, N., & Skopljak, F. (2017). Methane and
466 hydrogen in hyperalkaline groundwaters of the serpentized Dinaride ophiolite belt, Bosnia and
467 Herzegovina. *Applied Geochemistry*, 84, 286–296. <https://doi.org/10.1016/j.apgeochem.2017.07.006>
- 468 Etiope, G., Vadillo, I., Whiticar, M., Marques, J., Carreira, P., Tiago, I., Benavente, J., Jiménez, P., & Urresti,
469 B. (2015). Abiotic methane seepage in the Ronda peridotite massif, southern Spain. *Applied*
470 *Geochemistry*, 66, 101–113. <https://doi.org/10.1016/j.apgeochem.2015.12.001>
- 471 EuroGeoSurveys EGDI Operations Group. (2021, September 1). MIN4EU harmonized dataset – “Minerals
472 Inventory” [Web Map Service]. EGDI Spatial Metadata Catalogue. <https://www.europe-geology.eu/mineral-resources/>
- 473
- 474 Fejza, I., Avdullahi, S., Meshi, A., Meha, M., & Tmava, A. (2010). Ultrabasic Massif of Golesh (Kosova):
475 Microstructural and Kinematic Analysis. *Online Journal of Earth Sciences*, 4(1), 6–12.
476 <https://doi.org/10.3923/ojesci.2010.6.12>
- 477 Fejza, I., Shala, A., Kulllovci, F., & Tmava, A. (2022). Petrographic and geochemical characteristics of
478 rocks in the Drenas region, Kosovo. *Mining of Mineral Deposits*, 16(2), 110–115.
479 <https://doi.org/10.33271/mining16.02.110>
- 480 Flinn, D. (2001). The basic rocks of the Shetland Ophiolite Complex and their bearing on its genesis.
481 *Scottish Journal of Geology*, 37(2), 79–96. <https://doi.org/10.1144/sjg37020079>
- 482 Fraefel, M. (2008). Geomorphic response to neotectonic activity in the Jura Mountains and in the southern
483 Upper Rhine Graben. <https://doi.org/10.5451/unibas-004757231>
- 484 Frassi, C., Musumeci, G., Zucali, M., Mazzarini, F., Rebay, G., & Langone, A. (2017). The Cotoncello Shear
485 Zone (Elba Island, Italy): The deep root of a fossil oceanic detachment fault in the Ligurian ophiolites.
486 *Lithos*, 278–281, 445–463. <https://doi.org/10.1016/j.lithos.2017.02.015>
- 487 Frery, E., Langhi, L., Maison, M., & Moretti, I. (2021). Natural hydrogen seeps identified in the North Perth
488 Basin, Western Australia. *International Journal of Hydrogen Energy*, 46(61), 31158–31173.
489 <https://doi.org/10.1016/j.ijhydene.2021.07.023>
- 490 Fuel cell works. (2024, October 21). Natural hydrogen, helium found in Finland by 80 Mile Plc | Fuel Cells
491 works. <https://fuelcellsworks.com/2024/10/21/green-hydrogen/80-mile-plc-discovers-natural-hydrogen- helium-at-hammaslahti-project-in-finland>
- 492
- 493 Féménias, O., Coussaert, N., Bingen, B., Whitehouse, M., Mercier, J. C., & Demaiffe, D. (2003). A Permian
494 underplating event in late- to post-orogenic tectonic setting. Evidence from the mafic–ultramafic layered

- 495 xenoliths from Beaunit (French Massif Central). *Chemical Geology*, 199(3–4), 293–315.
496 [https://doi.org/10.1016/s0009-2541\(03\)00124-4](https://doi.org/10.1016/s0009-2541(03)00124-4)
- 497 Gaucher, E. C., Moretti, I., Pélissier, N., Burridge, G., & Gonthier, N. (2023). The place of natural hydrogen
498 in the energy transition: A position paper. Zenodo (CERN European Organization for Nuclear Research).
499 <https://doi.org/10.5281/zenodo.8108239>
- 500 Gee, D. G., & Stephenson, R. A. (2006). The European lithosphere: an introduction. *Geological Society
501 London Memoirs*, 32(1), 1–9. <https://doi.org/10.1144/gsl.mem.2006.032.01.01>
- 502 Gelman, S. E., Hearon, J. S., & Ellis, G. S. (2025). Prospectivity mapping for geologic hydrogen. USGS
503 Professional Paper. <https://doi.org/10.3133/pp1900>
- 504 George, R. P. (1978). Structural petrology of the Olympus ultramafic complex in the Troodos ophiolite,
505 Cyprus. *Geological Society of America Bulletin*, 89(6), 845. [https://doi.org/10.1130/0016-7606\(1978\)89](https://doi.org/10.1130/0016-7606(1978)89)
- 506 Gillard, M., Tugend, J., Müntener, O., Manatschal, G., Karner, G. D., Autin, J., Sauter, D., Figueredo, P. H., &
507 Ulrich, M. (2019). The role of serpentinization and magmatism in the formation of decoupling interfaces at
508 magma-poor rifted margins. *Earth-Science Reviews*, 196, 102882.
509 <https://doi.org/10.1016/j.earscirev.2019.102882>
- 510 González-Pérez, I., Fanlo, I., Ares, G., Gervilla, F., González-Jiménez, J. M., Acosta-Vigil, A., & Arranz, E.
511 (2023). The unconventional Peridotite-Related MG-FE-B Skarn of the El Robledal, SE Spain. *Minerals*,
512 13(3), 300. <https://doi.org/10.3390/min13030300>
- 513 Handy, M. R., Giese, J., Schmid, S. M., Pleuger, J., Spakman, W., Onuzi, K., & Ustaszewski, K. (2019).
514 Coupled Crust-Mantle response to slab tearing, bending, and rollback along the Dinaride-Hellenide
515 orogen. *Tectonics*, 38(8), 2803–2828. <https://doi.org/10.1029/2019tc005524>
- 516 Havlíček, F., Uličný, D., Krýza, O., Machek, M., Warsitzka, M., and Závada, P. (2024). Modelling the effects
517 of changing extension directions in a segmented rift: application to the Eger Rift, Central Europe, EGU
518 General Assembly 2024, Vienna, Austria, EGU24-9770, <https://doi.org/10.5194/egusphere-egu24-9770>
- 519 Heggie, G., Barnes, S., & Fiorentini, M. (2013). Application of lithogeochemistry in the assessment of
520 nickel-sulphide potential in komatiite belts from northern Finland and Norway. *Bulletin of the Geological
521 Society of Finland*, 85(2), 107–126. <https://doi.org/10.17741/bgsf/85.2.001>
- 522 Hunt, T. (1978). Interpretation of gravity anomalies over the Dun Mountain ultramafic body (Note). *New
523 Zealand Journal of Geology and Geophysics*, 21(3), 413–417.
524 <https://doi.org/10.1080/00288306.1978.10424065>
- 525 INSPIRE, Temporary MIWP 2021–2024 sub-group 2.3.1. (2024, July 31). D2.8.III.21 Data specification on
526 mineral resources – Technical guidelines (Version 3.0.0). INSPIRE Maintenance and Implementation
527 Group (MIG). <https://inspire.ec.europa.eu/id/document/tg/mr>
- 528 Jackson, O., Lawrence, S. R., Hutchinson, I. P., Stocks, A. E., Barnicoat, A. C., & Powney, M. (2024).
529 Natural hydrogen: sources, systems and exploration plays. *Geoenergy*, 2(1).
530 <https://doi.org/10.1144/geoenergy2024-002>
- 531 Jesus, A. P., Munhá, J., Mateus, A., Tassinari, C., & Nutman, A. P. (2007). The Beja Layered Gabbroic
532 Sequence (Ossa-Morena Zone, Southern Portugal): geochronology and geodynamic implications.
533 *Geodinamica Acta*, 20(3), 139–157. <https://doi.org/10.3166/ga.20.139-157>

- 534 Jin, Z., Zhang, P., Liu, R., Huang, X., Wang, X., Meng, Q., Liu, J., Su, Y., & Zhang, H. (2024). Discovery of
535 anomalous hydrogen leakage sites in the Sanshui Basin, South China. *Science Bulletin*, 69(9), 1217–
536 1220. <https://doi.org/10.1016/j.scib.2024.03.002>
- 537 Khogenkumar, S., Singh, A. K., Singh, R. B., Khanna, P., Singh, N. I., & Singh, W. I. (2015). Coexistence of
538 MORB and OIB-type mafic volcanics in the Manipur Ophiolite Complex, Indo-Myanmar Orogenic Belt,
539 northeast India: Implication for heterogeneous mantle source at the spreading zone. *Journal of Asian
540 Earth Sciences*, 116, 42–58. <https://doi.org/10.1016/j.jseaes.2015.11.007>
- 541 Klein, F., Bach, W., & McCollom, T. M. (2013). Compositional controls on hydrogen generation during
542 serpentinization of ultramafic rocks. *Lithos*, 178, 55–69. <https://doi.org/10.1016/j.lithos.2013.03.008>
- 543 Konnunaho, J., Hanski, E., Wing, B., Bekker, A., Lukkari, S., & Halkoaho, T. (2015). The Hietaharju PGE-
544 enriched komatiite-hosted sulfide deposit in the Archean Suomussalmi greenstone belt, eastern Finland.
545 *Ore Geology Reviews*, 72, 641–658. <https://doi.org/10.1016/j.oregeorev.2015.08.022>
- 546 Kousksou, T., Bruel, P., Jamil, A., Rhafiki, T. E., & Zeraouli, Y. (2013). Energy storage: Applications and
547 challenges. *Solar Energy Materials and Solar Cells*, 120, 59–80.
548 <https://doi.org/10.1016/j.solmat.2013.08.015>
- 549 Kryza, R., & Pin, C. (2009). The Central-Sudetic ophiolites (SW Poland): Petrogenetic issues,
550 geochronology and palaeotectonic implications. *Gondwana Research*, 17(2–3), 292–305.
551 <https://doi.org/10.1016/j.gr.2009.11.001>
- 552 Kumar, K. R., Makhmutov, A., Spiers, C. J., & Hajibeygi, H. (2021). Geomechanical simulation of energy
553 storage in salt formations. *Scientific Reports*, 11(1). <https://doi.org/10.1038/s41598-021-99161-8>
- 554 Kübler, S., Streich, R., Lück, E., Hoffmann, M., Friedrich, A. M., & Strecker, M. R. (2016). Active faulting in a
555 populated low-strain setting (Lower Rhine Graben, Central Europe) identified by geomorphic, geophysical
556 and geological analysis. *Geological Society London Special Publications*, 432(1), 127–146.
557 <https://doi.org/10.1144/sp432.11>
- 558 Langhi, L., & Strand, J. (2023b). Exploring natural hydrogen hotspots: a review and soil-gas survey design
559 for identifying seepage. *Geoenergy*, 1(1). <https://doi.org/10.1144/geoenergy2023-014>
- 560 Lefevre, N., Thomas, E., Truche, L., Donzé, F., Cros, T., Dupuy, J., Pinzon-Rincon, L., & Rigollet, C. (2024).
561 Characterizing natural hydrogen occurrences in the Paris Basin from historical drilling records.
562 *Geochemistry Geophysics Geosystems*, 25(5). <https://doi.org/10.1029/2024gc011501>
- 563 Lefevre, N., Truche, L., Donzé, F., Ducoux, M., Barré, G., Fakoury, R., Calassou, S., & Gaucher, E. C.
564 (2021). Native H₂ exploration in the western Pyrenean foothills. *Geochemistry Geophysics Geosystems*,
565 22(8). <https://doi.org/10.1029/2021gc009917>
- 566 Lefevre, N., Truche, L., Donzé, F., Gal, F., Tremosa, J., Fakoury, R., Calassou, S., & Gaucher, E. (2022).
567 Natural hydrogen migration along thrust faults in foothill basins: The North Pyrenean Frontal Thrust case
568 study. *Applied Geochemistry*, 145, 105396. <https://doi.org/10.1016/j.apgeochem.2022.105396>
- 569 Leshukov, T., Legoshchin, K., Avdeev, K., Baranova, E., & Larionov, A. (2024). Depth gradient and radon
570 activity concentration in soil gas in the zone of a potentially active fault. *Earth*, 5(4), 1005–1022.
571 <https://doi.org/10.3390/earth5040052>
- 572 Liebreich, M. (2023, October 20). Hydrogen Ladder Version 5.0. LinkedIn.
573 <https://www.linkedin.com/pulse/hydrogen-ladder-version-50-michael-liebreich>

- 574 Liipo, J., Vuollo, J., Nykänen, V., Piirainen, T., Pekkarinen, L., & Tuokko, I. (1995). Chromites from the early
575 Proterozoic Outokumpu-Jormua Ophiolite Belt: a comparison with chromites from Mesozoic ophiolites.
576 *Lithos*, 36(1), 15–27. [https://doi.org/10.1016/0024-4937\(95\)00002-w](https://doi.org/10.1016/0024-4937(95)00002-w)
- 577 Liu, J., Liu, Q., Xu, H., Ding, Q., Zhu, D., & Meng, Q. (2023). Genesis and energy significance of natural
578 hydrogen. *Unconventional Resources*, 3, 176–182. <https://doi.org/10.1016/j.uncres.2023.01.002>
- 579 Lollar, B. S., Onstott, T. C., Lacrampe-Couloume, G., & Ballentine, C. J. (2014). The contribution of the
580 Precambrian continental lithosphere to global H₂ production. *Nature*, 516(7531), 379–382.
581 <https://doi.org/10.1038/nature14017>
- 582 Lollar, B. S., Voglesonger, K., Lin, L., Lacrampe-Couloume, G., Telling, J., Abrajano, T., Onstott, T., & Pratt,
583 L. (2007). Hydrogeologic Controls on Episodic H₂ Release from Precambrian Fractured Rocks—Energy for
584 Deep Subsurface Life on Earth and Mars. *Astrobiology*, 7(6), 971–986.
585 <https://doi.org/10.1089/ast.2006.0096>
- 586 Lusty, P. A., Lacinska, A. M., Millar, I. L., Barrie, C. D., & Boyce, A. J. (2017b). Volcanological and
587 environmental controls on the Snowdon mineralization, North Wales, UK: A failed volcanogenic massive
588 sulfide system in the Avalon Zone of the British Caledonides. *Ore Geology Reviews*, 89, 557–586.
589 <https://doi.org/10.1016/j.oregeorev.2017.06.031>
- 590 Lévy, D., Boka-Mene, M., Meshi, A., Fejza, I., Guermont, T., Hauville, B., & Pelissier, N. (2023). Looking for
591 natural hydrogen in Albania and Kosova. *Frontiers in Earth Science*, 11.
592 <https://doi.org/10.3389/feart.2023.1167634>
- 593 Lévy, D., Roche, V., Pasquet, G., Combaudon, V., Geymond, U., Loiseau, K., & Moretti, I. (2023). Natural
594 H₂ exploration: tools and workflows to characterize a play. *Science and Technology for Energy Transition*,
595 78, 27. <https://doi.org/10.2516/stet/2023021>
- 596 Maier, W. D., Peltonen, P., Halkoaho, T., & Hanski, E. (2013). Geochemistry of komatiites from the
597 Tipasjärvi, Kuhmo, Suomussalmi, Ilomantsi and Tulppio greenstone belts, Finland: Implications for
598 tectonic setting and Ni sulphide prospectivity. *Precambrian Research*, 228, 63–84.
599 <https://doi.org/10.1016/j.precamres.2012.12.004>
- 600 Maiga, O., Deville, E., Laval, J., Prinzhofer, A., & Diallo, A. B. (2023). Characterization of the spontaneously
601 recharging natural hydrogen reservoirs of Bourakebougou in Mali. *Scientific Reports*, 13(1).
602 <https://doi.org/10.1038/s41598-023-38977-y>
- 603 Marescotti, P., Comodi, P., Crispini, L., Gigli, L., Zucchini, A., & Fornasaro, S. (2019). Potentially Toxic
604 Elements in Ultramafic Soils: A Study from Metamorphic Ophiolites of the Voltri Massif (Western Alps,
605 Italy). *Minerals*, 9(8), 502. <https://doi.org/10.3390/min9080502>
- 606 Marques, J. M., Neves, M. O., Miller, A. Z., Rocha, C., Vance, S., Christensen, L., Etiope, G., Carreira, P. M.,
607 & Suzuki, S. (2017). Water-rock Interaction Ascribed to Hyperalkaline Mineral Waters in the Cabeço de
608 Vide Serpentinized Ultramafic Intrusive Massif (Central Portugal). *Procedia Earth and Planetary Science*,
609 17, 646–649. <https://doi.org/10.1016/j.proeps.2016.12.173>
- 610 Marshak, S., & Van Der Pluijm, B. A. (2020). Tectonics of the continental interior in the United States. In
611 Elsevier eBooks (pp. 173–186). <https://doi.org/10.1016/b978-0-08-102908-4.00139-9>
- 612 Mart Zijp, Nelskamp, S., & Doornenbal, H. (2017, March 19). European Unconventional Oil and Gas
613 Assessment (EUOGA): Resource estimation of shale gas and shale oil in Europe.
614 https://www.researchgate.net/publication/320490073_European_Unconventional_Oil_and_Gas_Assess
615 [ment_EUOGA_Resource_estimation_of_shale_gas_and_shale_oil_in_Europe](https://www.researchgate.net/publication/320490073_European_Unconventional_Oil_and_Gas_Assess)

- 616 Matenco, L., Balázs, A., Nader, F. H., Haq, B. U., & Fodor, L. (2021). Advances in the understanding of
617 multi-scale and coupled evolution of orogens, sedimentary basins and the underlying lithosphere. *Global*
618 and Planetary Change, 208, 103689. <https://doi.org/10.1016/j.gloplacha.2021.103689>
- 619 Mathur, Y., Awosiji, V., Mukerji, T., Scheirer, A. H., & Peters, K. E. (2023). Soil geochemistry of hydrogen and
620 other gases along the San Andreas fault. *International Journal of Hydrogen Energy*, 50, 411–419.
621 <https://doi.org/10.1016/j.ijhydene.2023.09.032>
- 622 Małachowska, A., Łukasik, N., Mioduska, J., & Gębicki, J. (2022). Hydrogen Storage in Geological
623 Formations—The potential of salt caverns. *Energies*, 15(14), 5038. <https://doi.org/10.3390/en15145038>
- 624 McConnell, B., Riggs, N., & Fritschle, T. (2020). Tectonic history across the Iapetus suture zone in Ireland.
625 Geological Society London Special Publications, 503(1), 333–345. <https://doi.org/10.1144/sp503-2019-233>
- 627 Melcher, F., Meisel, T., Puhl, J., & Koller, F. (2002). Petrogenesis and geotectonic setting of ultramafic rocks
628 in the Eastern Alps: constraints from geochemistry. *Lithos*, 65(1–2), 69–112.
629 [https://doi.org/10.1016/s0024-4937\(02\)00161-5](https://doi.org/10.1016/s0024-4937(02)00161-5)
- 630 Meshi, A., Boudier, F., Nicolas, A., & Milushi, I. (2009). Structure and tectonics of lower crustal and upper
631 mantle rocks in the Jurassic Mirdita ophiolites, Albania. *International Geology Review*, 52(2–3), 117–141.
632 <https://doi.org/10.1080/00206810902823982>
- 633 Mikrut, J., Matusiak-Małek, M., Ceuleneer, G., Grégoire, M., & Onuzi, K. (2024). Melt-rock interaction as a
634 factor controlling evolution of chromite and olivine in dunite - case study from the Kukes Massif (Mirdita
635 ophiolite, Albania). *Journal of Geosciences*, 49–64. <https://doi.org/10.3190/jgeosci.386>
- 636 Minissale, A., Magro, G., Martinelli, G., Vaselli, O., & Tassi, G. (2000). Fluid geochemical transect in the
637 Northern Apennines (central-northern Italy): fluid genesis and migration and tectonic implications.
638 *Tectonophysics*, 319(3), 199–222. [https://doi.org/10.1016/s0040-1951\(00\)00031-7](https://doi.org/10.1016/s0040-1951(00)00031-7)
- 639 Miró, J., Manatschal, G., Cadenas, P., & Muñoz, J. A. (2021). Reactivation of a hyperextended rift system:
640 The Basque–Cantabrian Pyrenees case. *Basin Research*, 33(6), 3077–3101.
641 <https://doi.org/10.1111/bre.12595>
- 642 Moilanen, M., Hanski, E., Konnunaho, J., Yang, S., Törmänen, T., Li, C., & Zhou, L. (2018). Re-Os isotope
643 geochemistry of komatiite-hosted Ni-Cu-PGE deposits in Finland. *Ore Geology Reviews*, 105, 102–122.
644 <https://doi.org/10.1016/j.oregeorev.2018.12.007>
- 645 Mężyk, M., Malinowski, M., & Mazur, S. (2021). Structure of a diffuse suture between Fennoscandia and
646 Sarmatia in SE Poland based on interpretation of regional reflection seismic profiles supported by
647 unsupervised clustering. *Precambrian Research*, 358, 106176.
648 <https://doi.org/10.1016/j.precamres.2021.106176>
- 649 Nance, R. D., Gutiérrez-Alonso, G., Keppie, J. D., Linnemann, U., Murphy, J. B., Quesada, C., Strachan, R.
650 A., & Woodcock, N. H. (2009). Evolution of the Rheic Ocean. *Gondwana Research*, 17(2–3), 194–222.
651 <https://doi.org/10.1016/j.gr.2009.08.001>
- 652 Nenakhov, V. M., Polevanov, V. P., Zhabin, A. V., Bondarenko, S. V., & Zolotareva, G. S. (2023). Prospects for
653 the discovery of natural hydrogen in the Voronezh antecline. *Doklady Earth Sciences*, 513(S2), S182–
654 S192. <https://doi.org/10.1134/s1028334x23603474>
- 655 Parnell, J., & Blamey, N. (2017). Global hydrogen reservoirs in basement and basins. *Geochemical*
656 *Transactions*, 18(1). <https://doi.org/10.1186/s12932-017-0041-4>

- 657 Passaro, S., Tamburrino, S., Vallefuoco, M., Tassi, F., Vaselli, O., Giannini, L., Chiodini, G., Caliro, S.,
658 Sacchi, M., Rizzo, A. L., & Ventura, G. (2016). Seafloor doming driven by degassing processes unveils
659 sprouting volcanism in coastal areas. *Scientific Reports*, 6(1). <https://doi.org/10.1038/srep22448>
- 660 Pawlewicz, M. J., Williams, A. J., Walden, S. M., Steinshouer, D. W., & Gautier, D. (2003). *Geology of*
661 Europe including Turkey [Data set]. U.S. Geological Survey, Central Energy Resources Team.
662 <https://doi.org/10.5066/P9C8ZY5Q>
- 663 Peltonen, P., & Kontinen, A. (2004b). The Jormua Ophiolite: a Mafic-Ultramafic Complex from an Ancient
664 Ocean-Continent Transition Zone. In *Developments in precambrian geology* (pp. 35–71).
665 [https://doi.org/10.1016/s0166-2635\(04\)13001-6](https://doi.org/10.1016/s0166-2635(04)13001-6)
- 666 Petrović, D., Cvetkov, V., Vasiljević, I., & Cvetković, V. (2015). A new geophysical model of the Serbian part
667 of the East Vardar ophiolite: Implications for its geodynamic evolution. *Journal of Geodynamics*, 90, 1–13.
668 <https://doi.org/10.1016/j.jog.2015.07.003>
- 669 Pin, C., Fonseca, P. E., Paquette, J., Castro, P., & Matte, P. (2008). The ca. 350 Ma Beja Igneous Complex: A
670 record of transcurrent slab break-off in the Southern Iberia Variscan Belt? *Tectonophysics*, 461(1–4), 356–
671 377. <https://doi.org/10.1016/j.tecto.2008.06.001>
- 672 Pin, C., Paquette, J. L., Ábalos, B., Santos, F. J., & Ibarguchi, J. I. G. (2006). Composite origin of an early
673 Variscan transported suture: Ophiolitic units of the Morais Nappe Complex (north Portugal). *Tectonics*,
674 25(5). <https://doi.org/10.1029/2006tc001971>
- 675 Pitkänen, P., Ahokas, H., Ylä-Mella, M., Partamies, S., Snellman, M., & Hellä, P. (2007). Quality Review of
676 Hydrochemical Baseline Data from the Olkiluoto Site. Posiva. Posiva Report No. 2007-5
- 677 Plissart, G., Monnier, C., Diot, H., Mărunțiu, M., Berger, J., & Triantafyllou, A. (2017). Petrology,
678 geochemistry and Sm-Nd analyses on the Balkan-Carpathian Ophiolite (BCO – Romania, Serbia,
679 Bulgaria): Remnants of a Devonian back-arc basin in the easternmost part of the Variscan domain.
680 *Journal of Geodynamics*, 105, 27–50. <https://doi.org/10.1016/j.jog.2017.01.001>
- 681 Pomonis, P., & Maggnas, A. (2017). Petrogenetic Implications for Ophiolite Ultramafic Bodies from Lokris
682 and Beotia (Central Greece) Based on Chemistry of Their Cr-spinels. *Geosciences*, 7(1), 10.
683 <https://doi.org/10.3390/geosciences7010010>
- 684 Prevorcic, R. (2014). Die Geologie des Kraubather Ultramafitkomplexes zwischen Wintergraben und
685 Lobminggraben (Steiermark, Österreich). Leoben University.
686 <https://pure.unileoben.ac.at/portal/files/4425234/AC12181454n01.pdf>
- 687 Prinzhöfer, A., Moretti, I., Françolin, J., Pacheco, C., D'Agostino, A., Werly, J., & Rupin, F. (2019). Natural
688 hydrogen continuous emission from sedimentary basins: The example of a Brazilian H₂-emitting
689 structure. *International Journal of Hydrogen Energy*, 44(12), 5676–5685.
690 <https://doi.org/10.1016/j.ijhydene.2019.01.119>
- 691 Puga, E., De Federico, A. D., Fanning, M., Nieto, J., Martínez-Conde, J. R., Puga, M. D., Lozano, J.,
692 Bianchini, G., Natali, C., & Beccaluva, L. (2017). The Betic ophiolites and the mesozoic evolution of the
693 Western Tethys. *Geosciences*, 7(2), 31. <https://doi.org/10.3390/geosciences7020031>
- 694 Putić, M., Nemec, O., Ustalić, S., Babajić, E., Ružička, P., Koller, F., Kurylo, S., & Katanić, P. (2022).
695 Mineralogical-Petrographical Record of Melt-Rock Interaction and P-T Estimates from the Ozren Massif
696 Ophiolites (Bosnia and Herzegovina). *Minerals*, 12(9), 1108. <https://doi.org/10.3390/min12091108>

- 697 Pál-Molnár, E., Batki, A., Almási, E., Kiss, B., Upton, B. G., Markl, G., Odling, N., & Harangi, S. (2015).
698 Origin of mafic and ultramafic cumulates from the Ditrău Alkaline Massif, Romania. *Lithos*, 239, 1–18.
699 <https://doi.org/10.1016/j.lithos.2015.09.022>
- 700 Randazzo, P., Caracausi, A., Aiuppa, A., Cardellini, C., Chiodini, G., D'Alessandro, W., Vigni, L. L., Papic,
701 P., Marinkovic, G., & Ionescu, A. (2021). Active degassing of deeply sourced fluids in central Europe: new
702 evidences from a geochemical study in Serbia. *Geochemistry Geophysics Geosystems*, 22(11).
703 <https://doi.org/10.1029/2021gc010017>
- 704 Rattey, R. P., & Hayward, A. B. (1993). Sequence stratigraphy of a failed rift system: the Middle Jurassic to
705 Early Cretaceous basin evolution of the Central and Northern North Sea. *Geological Society London*
706 *Petroleum Geology Conference Series*, 4(1), 215–249. <https://doi.org/10.1144/0040215>
- 707 Ring, U., & Pantazides, H. (2019). The uplift of the Troodos Massif, Cyprus. *Tectonics*, 38(8), 3124–3139.
708 <https://doi.org/10.1029/2019tc005514>
- 709 Rizzo, A. L., Barberi, F., Carapezza, M. L., Di Piazza, A., Francalanci, L., Sortino, F., & D'Alessandro, W.
710 (2015). New mafic magma refilling a quiescent volcano: Evidence from He-Ne-Ar isotopes during the
711 2011–2012 unrest at Santorini, Greece. *Geochemistry Geophysics Geosystems*, 16(3), 798–814.
712 <https://doi.org/10.1002/2014gc005653>
- 713 Roberts, D., Nilsson, L. P., & Ramsay, D. M. (2005). The Raudfjellet ophiolite fragment, Central Norwegian
714 Caledonides: principal lithological and structural features. <https://hdl.handle.net/11250/2674161>
- 715 Rohrman, M., Van Der Beek, P., & Andriessen, P. (1994). Syn-rift thermal structure and post-rift evolution
716 of the Oslo Rift (southeast Norway): New constraints from fission track thermochronology. *Earth and*
717 *Planetary Science Letters*, 127(1–4), 39–54. [https://doi.org/10.1016/0012-821x\(94\)90196-1](https://doi.org/10.1016/0012-821x(94)90196-1)
- 718 Rosberg, J., & Erlström, M. (2021). Evaluation of deep geothermal exploration drillings in the crystalline
719 basement of the Fennoscandian Shield Border Zone in south Sweden. *Geothermal Energy*, 9(1).
720 <https://doi.org/10.1186/s40517-021-00203-1>
- 721 Roux, V. L., Bodinier, J., Tommasi, A., Alard, O., Dautria, J., Vauchez, A., & Riches, A. (2007). The Lherz
722 spinel lherzolite: Refertilized rather than pristine mantle. *Earth and Planetary Science Letters*, 259(3–4),
723 599–612. <https://doi.org/10.1016/j.epsl.2007.05.026>
- 724 Saccani, E., Nicolae, I., & Tassinari, R. (2001). TECTONO-MAGMATIC SETTING OF THE JURASSIC
725 OPHIOLITES FROM THE SOUTH APUSENI MOUNTAINS (ROMANIA): PETROLOGICAL AND GEOCHEMICAL
726 EVIDENCE. *Ophioliti*, 26(1), 9–22. <https://doi.org/10.4454/ophioliti.v26i1.127>
- 727 Sano, S. (2002). Petrological, geochemical and isotopic constraints on the origin of the Harzburg
728 intrusion, Germany. *Journal of Petrology*, 43(8), 1529–1549. <https://doi.org/10.1093/petrology/43.8.1529>
- 729 Saspiturry, N., Allanic, C., & Peyrefitte, A. (2024). Serpentinitization and magmatic distribution in a
730 hyperextended rift suture: Implication for natural hydrogen exploration (Mauléon Basin, Pyrenees).
731 *Tectonics*, 43(8). <https://doi.org/10.1029/2024tc008385>
- 732 Schaltegger, U., Abrecht, J., & Corfu, F. (2003). The Ordovician orogeny in the Alpine basement:
733 constraints from geochronology and geochemistry in the Aar Massif (Central Alps). *Schweizerische*
734 *Mineralogische Und Petrographische Mitteilungen*, 83, 183–195. <https://archive-ouverte.unige.ch/unige:28437>
- 736 Schovsbo, N. H., Doornenbal, H., Nelkamp, S., Pedersen, C. B., Tougaard, L., Zijp, M., & Anthonsen, K. L.
737 (2017). Review of results and recommendations. Delivery T8 of the EUOGA study (EU Unconventional Oil

- 738 and Gas Assessment) commissioned by JRC-IET. European Commission.
739 <https://doi.org/10.22008/FK2/4JS6NW/6RLA3Z>
- 740 Segvic, B. (2010). Petrologic and geochemical characteristics of the Krivaja-Konjuh ophiolite complex (NE
741 Bosnia and Herzegovina) - petrogenesis and regional geodynamic implications.
742 <https://doi.org/10.11588/heidok.00010432>
- 743 Slagstad, T., Pin, C., Roberts, D., Kirkland, C. L., Grenne, T., Dunning, G., Sauer, S., & Andersen, T. (2013).
744 Tectonomagmatic evolution of the Early Ordovician suprasubduction-zone ophiolites of the Trondheim
745 Region, Mid-Norwegian Caledonides. Geological Society London Special Publications, 390(1), 541–561.
746 <https://doi.org/10.1144/sp390.11>
- 747 Smit, J., Van Wees, J., & Cloetingh, S. (2016). The Thor suture zone: From subduction to intraplate basin
748 setting. Geology, 44(9), 707–710. <https://doi.org/10.1130/g37958.1>
- 749 Smith, N. J. P., Shepherd, T. J., Styles, M. T., & Williams, G. M. (2005). Hydrogen exploration: a review of
750 global hydrogen accumulations and implications for prospective areas in NW Europe. Geological Society
751 London Petroleum Geology Conference Series, 6(1), 349–358. <https://doi.org/10.1144/0060349>
- 752 Sreckovic-Batocanin, D., Vaskovic, N., Matovic, V., & Gajic, V. (2012). Correlation of metabasic rocks from
753 metamorphic soles of the Dinaridic and the Western Vardar zone ophiolites (Serbia): Three contrasting
754 pressure-temperature-time paths. Geoloski Analji Balkanskog Poluostrva, 73, 61–85.
755 <https://doi.org/10.2298/gabp1273061s>
- 756 Stober, I., Teiber, H., Li, X., Jendryszczyk, N., & Bucher, K. (2017). Chemical composition of surface- and
757 groundwater in fast-weathering silicate rocks in the Seiland Igneous Province, North Norway. Norwegian
758 Journal of Geology. <https://doi.org/10.17850/njg97-1-04>
- 759 Suberu, M. Y., Mustafa, M. W., & Bashir, N. (2014). Energy storage systems for renewable energy power
760 sector integration and mitigation of intermittency. Renewable and Sustainable Energy Reviews, 35, 499–
761 514. <https://doi.org/10.1016/j.rser.2014.04.009>
- 762 Séjourné, S., Comeau, F., Santos, M. L. M. D., Bordeleau, G., Claproot, M., Mouge, P., Mulliez, V., Malo,
763 M., Giroux, B., Gloaguen, E., & Raymond, J. (2024). Potential for natural hydrogen in Quebec (Canada): a
764 first review. Frontiers in Geochemistry, 2. <https://doi.org/10.3389/fgeoc.2024.1351631>
- 765 Templeton, A. S., Ellison, E. T., Kelemen, P. B., Leong, J., Boyd, E. S., Colman, D. R., & Matter, J. M. (2024).
766 Low-temperature hydrogen production and consumption in partially-hydrated peridotites in Oman:
767 implications for stimulated geological hydrogen production. Frontiers in Geochemistry, 2.
768 <https://doi.org/10.3389/fgeoc.2024.1366268>
- 769 Tremblay, A., Meshi, A., Deschamps, T., Goulet, F., & Goulet, N. (2015). The Vardar zone as a suture for the
770 Mirdita ophiolites, Albania: Constraints from the structural analysis of the Korabi-Pelagonia zone.
771 Tectonics, 34(2), 352–375. <https://doi.org/10.1002/2014tc003807>
- 772 Truche, L., Donzé, F., Goskolli, E., Muceku, B., Loisy, C., Monnin, C., Dutoit, H., & Cerepi, A. (2024). A deep
773 reservoir for hydrogen drives intense degassing in the Bulqizë ophiolite. Science, 383(6683), 618–621.
774 <https://doi.org/10.1126/science.adk9099>
- 775 Tugend, J., Manatschal, G., Kusznir, N. J., Masini, E., Mohn, G., & Thinon, I. (2014). Formation and
776 deformation of hyperextended rift systems: Insights from rift domain mapping in the Bay of Biscay-
777 Pyrenees. Tectonics, 33(7), 1239–1276. <https://doi.org/10.1002/2014tc003529>

- 778 Uliasz-Misiak, B., Lewandowska-Śmierzchalska, J., Matuła, R., & Tarkowski, R. (2022). Prospects for the
779 implementation of underground hydrogen storage in the EU. *Energies*, 15(24), 9535.
780 <https://doi.org/10.3390/en15249535>
- 781 Ustalić, S., Nemec, O., Milovská, S., Putiš, M., Babajić, E., Kurylo, S., & Ružička, P. (2024). Amphibole
782 group minerals in the Ozren Massif ophiolites of Bosnia and Herzegovina as petrogenetic indicators.
783 *Minerals*, 14(3), 239. <https://doi.org/10.3390/min14030239>
- 784 Utley, J. (2025, March 3). Natural hydrogen – the treasure hidden underground | FAU Erlangen-Nürnberg.
785 FAU Erlangen-Nürnberg. [https://www.fau.eu/2024/11/news/natural-hydrogen-the-treasure-hidden-](https://www.fau.eu/2024/11/news/natural-hydrogen-the-treasure-hidden-underground)
786 [underground](#)
- 787 Virtanen, V. J., Höytiä, H. M., Iacono-Marziano, G., Yang, S., Moilanen, M., & Törmänen, T. (2024). From the
788 mantle source to the crustal sink: magmatic differentiation and sulfide saturation of the Paleoproterozoic
789 komatiites of the Central Lapland Greenstone Belt, Finland. *Contributions to Mineralogy and Petrology*,
790 179(7). <https://doi.org/10.1007/s00410-024-02154-9>
- 791 Wang, L., Jin, Z., Chen, X., Su, Y., & Huang, X. (2023). The origin and occurrence of natural hydrogen.
792 *Energies*, 16(5), 2400. <https://doi.org/10.3390/en16052400>
- 793 Wybraniec, S., Zhou, S., Thybo, H., Forsberg, R., Perchuc, E., Lee, M., Demianov, G. D., & Strakhov, V. N.
794 (1998). New map compiled of Europe's gravity field. *Eos*, 79(37), 437–442.
795 <https://doi.org/10.1029/98eo00330>
- 796 Wójcik, K. (2024). Wódór naturalny w Polsce. *Przegląd Geologiczny*, 72(10), 584–596.
797 <https://doi.org/10.7306/2024.37>
- 798 Xiang, Y., Sun, X., Liu, D., Yan, L., Wang, B., & Gao, X. (2020). Spatial distribution of RN, CO₂, HG, and H₂
799 concentrations in soil gas across a thrust fault in Xinjiang, China. *Frontiers in Earth Science*, 8.
800 <https://doi.org/10.3389/feart.2020.554924>
- 801 Xiong, F., Yang, J., Robinson, P. T., Dilek, Y., Milushi, I., Xu, X., Chen, Y., Zhou, W., Zhang, Z., Lai, S., Tian, Y.,
802 & Huang, Z. (2015). Petrology and geochemistry of high Cr# podiform chromitites of Bulqiza, Eastern
803 Mirdita Ophiolite (EMO), Albania. *Ore Geology Reviews*, 70, 188–207.
804 <https://doi.org/10.1016/j.oregeorev.2015.04.011>
- 805 Zgonnik, V. (2020). The occurrence and geoscience of natural hydrogen: A comprehensive review. *Earth-
806 Science Reviews*, 203, 103140. <https://doi.org/10.1016/j.earscirev.2020.103140>
- 807 Zgonnik, V., Beaumont, V., Deville, E., Larin, N., Pillot, D., & Farrell, K. M. (2015). Evidence for natural
808 molecular hydrogen seepage associated with Carolina bays (surficial, ovoid depressions on the Atlantic
809 Coastal Plain, Province of the USA). *Progress in Earth and Planetary Science*, 2(1).
810 <https://doi.org/10.1186/s40645-015-0062-5>
- 811 Zuo, J., Webb, A. a. G., Chin, E. J., Ackerman, L., Harvey, J., Haproff, P. J., Müller, T., Wang, Q., Hickman, A.
812 H., Sorger, D., & Ramírez-Salazar, A. (2022). Earth's Earliest Phaneritic Ultramafic Rocks: Mantle Slices or
813 Crustal Cumulates? *Geochemistry Geophysics Geosystems*, 23(12).
814 <https://doi.org/10.1029/2022gc010519>
- 815 Zwaan, F., Brune, S., Glerum, A. C., Vasey, D. A., Naliboff, J. B., Manatschal, G., & Gaucher, E. C. (2025).
816 Rift-inversion orogens are potential hot spots for natural H₂ generation. *Science Advances*, 11(8).
817 <https://doi.org/10.1126/sciadv.adr3418>
- 818